Fractal-like overturning maps for stacked rocking blocks with numerical and experimental validation

Sokratis Anagnostopoulos, sa14970@bristol.ac.uk, 3 Byron Place, BS8 1EY, Bristol
Department of Mechanical Engineering, University of Bristol, UK

James Norman, james.norman@bristol.ac.uk
Department of Civil Engineering, University of Bristol, UK

George Mylonakis[1], g.mylonakis@bristol.ac.uk
Department of Civil Engineering, University of Bristol UK

Abstract: A novel, compact mathematical formulation is presented to describe the dynamic rocking response of single and double block systems subjected to gravity and/or ground excitation. The derivation of the closed-form solutions for impact and motion is based on the Euler-Lagrange equation and the conservation of angular momentum, and combines all the different cases of possible block relative rotating and impact modes (16 in total) into a single set of equations without the need of transient expressions. The derived equations that describe the impact modes are the equivalent to the expression derived by Housner and depend on the angular velocity of the blocks before impact. The analytical model is integrated numerically via an ad hoc algorithm and its reliability & accuracy are verified after various self-consistency tests and comparisons with the literature. In addition, several shaking table experiments were conducted in EQUALS laboratory in Bristol, set-up constructed to test free and forced rocking motion of single and double block configurations. The error margins of the measurements are determined, and the extracted data are in good agreement with the numerical results for most examined cases. The ideal Housner restitution coefficient of single block impact to a rigid base is adjusted to match experimental conditions, and it is found to be correlated with the block aspect ratio. The forced rocking of a two-block system is shown to exhibit numerous different response patterns depending on the excitation conditions. The integrated model is finally applied to produce normalised overturning maps for double block systems, subjected to single-pulse sine inputs, which uncover the existence of a fractal-type behaviour. This previously unsuspected trait of multi-block systems is reminiscent of the chaotic behaviour exhibited by a classical double pendulum and suggests that the risk of overturning can only be evaluated on a probabilistic sense.

Keywords: *Rocking rigid blocks; Stacked blocks; Dynamic response; Compact formulation; Euler-Lagrange equation; Restitution coefficient; Analytical model of motion and impacts; Laboratory measurements of free and excited blocks; Overturning maps*

[1] Corresponding author

1 Introduction

For millennia, free-standing rigid blocks have been used as structural components in construction. Modular structures in which a large block is placed on top of a block-like pedestal have been extensively used in ancient architecture, even though their seismic behaviour was probably not well understood, as they do not develop high shear stresses under gravity and/or external dynamic disturbances [1, 2]. However, structures made of unanchored blocks are prone to overturning, which can have catastrophic effects during an earthquake.

From shipping containers, modular construction projects and houses in less developed countries, to monuments like Stonehenge and the Parthenon, and modern free founded block-structures (oil storage tanks, water towers, nuclear reactors, machines, computer equipment, furniture and many artefacts), the rocking block problem has been a challenge of past and modern mechanics. While past empirical methods used to design such structures have been considerably developed, the modelling and analysis tools that are available today provide great capabilities for better understanding, predicting and improving the behaviour of a single block or a modular configuration under seismic excitation.

The dynamics of a single rocking block has intrigued a great number of researchers, including seismologists and engineers over the years, and numerous academic papers have been published as a result [3-35]. Early observations and studies go back to the late 19th and the first half of the 20th century [3-7]. The first simple model estimating the effect of impact on the rocking motion of a rigid body (energy dissipation and new angular velocity), was derived by Housner [8] based on the principle of angular momentum conservation. This theoretical approach is being widely used today, though it refers to idealised impact conditions and block geometries. Aslam [10] studied the rocking and overturning response of various blocks under strong earthquake accelerations, and the behaviour of vertically anchored blocks to the floor. Ishiyama [12] derived the equations of six motion types of a rigid body and determined a horizontal (in addition to vertical) restitution coefficient during impact, to simulate the motion and study the overturning behaviour of a body subjected to sinusoidal and earthquake excitations.

Over the last 20 years, several researchers [15-35] studied the rocking response and overturning behaviour of single rigid blocks subjected to idealised pulses and real or artificial earthquake excitations, using in most cases numerical tools to integrate the equations of motion. Makris & Roussos [15] showed that a block may overturn during its free-vibration regime (not simply during an imposed pulse) and developed an overturning criterion referring to an infinite time after the end of excitation. More precise overturning criteria were later defined by Voyagaki *et al.* [31-32] and Dimitrakopoulos & Fung [33].

Departing from the classical formulation by Housner, Pena *et al*. [19] used the Complex Coupled Rocking Rotations approach and the Discrete Element method to simulate the dynamic response of rocking blocks. The numerical results for free rocking motion were not in full agreement with the corresponding experimental data obtained in the same study, and hence appropriate fitting parameters (e.g. for the damping rate) were introduced to the numerical models to improve the agreement.

Zhang & Makris [16] examined the transient dynamics of the rocking block under sinusoidal ground excitations using semi-analytical and numerical solutions. They demonstrated that for a given restitution coefficient, the response and overturning behaviour of a slender rectangular block can be determined based on two dimensionless parameters: block slenderness relative to dimensionless peak ground acceleration, and a frequency ratio. They also showed that overturning can take place in two distinct modes (with and without impact) and defined the

corresponding regimes in slenderness-frequency ratio space. This study was later extended by Dimitrakopoulos & DeJong [29] who derived nearly-exact closed-form solutions based on series expansions of the relevant transcendental equations, and explored similarity laws and novel orientational analysis concepts.

An alternative pair of dimensionless governing parameters (namely uplift strength and pulse duration) were introduced by Voyagaki [30] and Voyagaki *et al.* [31-32] to describe the response of a rectangular block subjected to generalised ground acceleration pulses. These studies also investigated the effects of full-cycle and half-cycle pulses on the response and the overturning of the block with and without impact. The authors compared results between the linearised and the fully non-linear equations of motion, and employed a wide variety of pulse shapes and real recorded ground motions.

Prieto and Lourenco [36, 37], presented an alternative approach in order to derive a single differential equation to describe the rocking and impacting motion of a single block, by modelling the impact forces as Dirac-delta type interactions, and assuming a constant restitution coefficient. The results of the model show a good correlation with the analytic solution for a small slender angle tested, and using a sufficiently small value of an introduced motion coefficient [36].

The rocking instability and overturning modes of rectangular rigid blocks subjected to ground harmonic pulses were parametrically studied by Kounadis [33-34], by including and excluding sliding interaction, respectively.

The effect of harmonic excitation on the dynamic behavior of a rocking block has been examined by Hogan [38, 39], based on the orbital stability theory. Among others, he showed that above a maximum excitation amplitude, asymmetric orbits with non-periodic or chaotic behavior appear. Based on similar Poincaré Surface of Section Analysis, Prieto [37] carried out an extensive numerical study of the stability and the dynamic behavior for the harmonic forcing of a single block in the amplitude-frequency space. They also found that there are certain areas of strong sensitivity to both the initial conditions and the system parameters. For given parameter value, a pair of initially nearby states may diverge if a bifurcation is present [37].

Going beyond the single block, Makris & Vassiliou [2] explored the rocking response of an array of freestanding columns capped with a freely supported rigid beam, as a generalised single-degree-of-freedom problem. The analytical investigation showed that the top-beam makes the rocking frame more stable, despite rising the centre of mass.

With reference to two stacked blocks, an early attempt to develop a detailed analytical model for the relevant rocking motion was made by Psycharis [40], who employed Newtons's second law and assumed small rotation angles to derive eight sets of linearised dynamic equations to describe the corresponding rocking modes. The study showed that six equations govern the transition from one mode to another, after an impact, based on conservation of angular momentum, and eight equations govern the initiation of the various rocking modes. The equations were numerically integrated by a special algorithm to study the free vibrations and earthquake response of the system.

Spanos *et al.* [41] derived similar analytical expressions for the rocking patterns of two stacked blocks using the Euler-Lagrange equation. They also developed an impact model based on the conservation of angular momentum, which, again, is expressed for each of the several possible impacting modes of the blocks, along with additional transition conditions from one pattern to another, that complicates further the analysis. The authors simulate the system by a numerical algorithm and employ a 4^{th}-order Runge-Kutta method for time integration in order to produce

indicative numerical results for free rocking and for a horizontal earthquake excitation of the system.

A number of researchers investigated the seismic response of classical monuments (multi-drum columns and other megalithic structures) that are constructed in a modular manner [42-51]. Papastamatiou & Psycharis [43] used piece-wise linear equations to model the rocking of classical columns, and found that a modular column behaves like a system of two-blocks but the number of drums depends on the external excitation. Mouzakis *et al*. [48] carried out experiments on the earthquake response of a classical marble column model of the Parthenon, and found that its response is very sensitive to the initial conditions of the experiments, or to any imperfections in the geometry of the blocks. They concluded that their measurements cannot be repeatable, since the same experimental conditions produced different results after repeated tests. Similar sensitivity and non-repeatability is also reported in the experimental study of Bachmann et al. [62], leading to an impression that the seismic response of the rocking oscillator is chaotic.

For low excitation frequencies, Papaloizou & Komodromos [53] show that a multi-drum column behaves like a single block, but sliding motion is also triggered as the excitation frequency increases.

Some more complex cases of free-rocking response of rigid blocks have also been studied: a block standing on a seismically isolated base [20], a block at the top of an elastically restrained cantilever [58], analysis of rocking frames [63, 64], the rocking of a 3D body with a rectangular base [59], and the rocking response of a block on a nonlinear flexible foundation [66].

One of the key parameters dictating the response of multi block assemblies is the coefficient of restitution and the way it is treated in the solution. Experimental investigations of the response of rocking blocks to ground excitation are available in literature [7, 10, 11, 17, 19, 35]. ElGawady *et al*. [62] provide experimental results on the response of rigid blocks with aspect ratio 1:5, studying the effect of the interface material. The restitution coefficient obtained by the model of Housner was close to the measured one for concrete bases, but significantly different for rubber bases.

Extensive experimental work was carried out by Pena *et al*. [19], who studied the free rocking and the dynamic response of various granite stones subjected to different excitations on a shaking table. They carried out a more comprehensive study [51], in which they investigated experimentally the rocking behaviour of three types of free-standing structures: various single blocks, two stacked blocks, and a system of two parallel blocks capped by a third one. The repeatability for harmonic ground excitation was good for single blocks, but low for the stacked block response, which was found to be sensitive to the initial conditions. The effect of specimen imperfections (e.g. damaged corners) or insufficient contact and sliding in multi-block structures was also studied in order to identify limitations in predicting the response of real blocks.

Recently, Kalliontzis *et al*. [68] studied experimentally the free vibration rocking motion of three concrete blocks. To adjust their results, they propose to correct the classical Housner restitution model that underestimates the experimental observations. The derivation is based on the assumption that the impacting block rotates with respect to points that are close to, but not exactly at, its bottom corners. Spanos *et al*. [66] also carried out experiments of free rocking motion of rigid blocks on various flexible foundation materials, and used the measurements to validate their nonlinear impact force model.

The Euler-Lagrange equation is used in multi-block studies to produce the second order non-linear governing differential equation with respect to the angle θ of the block [69]. However,

as the number of blocks increases, the spectrum of the scientific research in this direction becomes narrow. From the analytical formulation in the publication of Minafo *et al.* [59] it emerges that the analysis of stacked rigid block systems becomes highly complex as the number of blocks increases, because the number of different rocking patterns increases very quickly. The authors numerically integrated the nonlinear differential equations for a system of three blocks, using a constant value for the restitution coefficient for all impact types.

In a more recent paper, Kounadis *et al*. [58] analysed the overturning instability of a two-block system under sinusoidal ground excitation, using the same sets of rocking motion expressions derived from the Euler-Lagrange equation, whereas the new angular velocities after an impact are simply obtained by assuming a 5% reduction in kinetic energy of the impacting block. They identify excitation frequency ranges for overturning with or without previous impacts, and found that for certain frequency values the two-block system becomes less stable than a single equivalent block.

Baratta & Corbi [21] introduced a distributional expression of the displacement impulsive reactions to derive a unified formulation of the equations of the rocking motion of a rigid body under dynamic excitation, treating damping effects as a consequence of the impulsive forces. Schau & Johannes [70] applied the Finite Element method to compare its predictions with results from the numerical integration of the analytic equations of free rocking motion. The FE analysis showed that any variation from the ideal rectangular geometry of the block cause higher restitution coefficients than those obtained by Housner's model. Casapulla & Maione [71] introduced a new formulation, with which the free damped vibrations of slender rigid blocks can be represented by a succession of uniformly accelerated/decelerated motions, using a variable restitution coefficient to account for various damping effects.

The three-block rocking system has also been investigated by Kounadis, where the piece-wise equations of motion were derived [72], [73] and the effect of sliding in the stability of the system as the number of blocks increase was proposed [73]. In a more recent work by the same author [74], the dynamic equations of motion of N-spondyle columns including the effect of small slips was derived. The effect of small slips was also correlated to the stability of columns; it was shown that the higher a statue is placed on a column (and the heavier it is) the more stable the system becomes due to the increasing loss of energy from bottom to top. These results were also supported experimentally.

The present work aims at deriving a unified system of governing equations capable of describing all possible rocking and impact modes of a single or two-stacked rigid blocks, based on the Euler-Lagrange approach and the conservation of angular momentum principle. This formulation does not need transient expressions and can, therefore, be efficiently programmed and computed. To this end, an ad-hoc computer algorithm was developed for the numerical modelling of rigid blocks response under free and forced rocking motion, and it was used to reproduce and study the behaviour of single and two-stacked blocks. Also, an experimental study was designed and performed at the University of Bristol shaking table (EQUALS laboratory), in order to measure the free and forced rocking motion of single and two-block systems and validate the reliability of the corresponding predictions. The resulting overturning maps demonstrate a previously unsuspected fractal pattern which can be interpreted in the context of deterministic chaos.

2 Materials and Methods

2.1 Problem description

The fundamental motion stages that describe the displacement of rectangular rigid bodies (blocks) in space are the following: translation, rotation (rocking), sliding and rest [40], [70]. Combinations can also occur where each motion can be described separately.

Several assumptions are usually made for the theoretical analysis of single or combined blocks motion, which are also adopted in the present work. Specifically:

1. The blocks are perfect rectangles.
2. The block and the base are rigid.
3. There is no bouncing or complete lifting ("upthrow") of the body.
4. Blocks are assumed not to be sliding on the ground or relative to each other.
5. Material stiffness and damping are not considered. In other words, the blocks cannot be compressed nor store/dissipate elastic energy.
6. Energy loss at impact is proportional to a coefficient of restitution (r).
7. The impact occurs at a single point (point of contact or rocking pole), which is a corner of the block.
8. The impact lasts for an infinitely small time interval.
9. The model is simplified for a 2-D geometry since there is no translational motion on the z-axis (Figure 1).

A typical block-base system is shown in Figure 1, where the symbols used for each parameter of a single block are depicted and explained in Table 1. Note that the same symbols will be used for the case of two blocks as well, with the appropriate index denoting the number of the block: 1 for the lower and 2 for the upper block. In that case, the two blocks can have different height and mass.

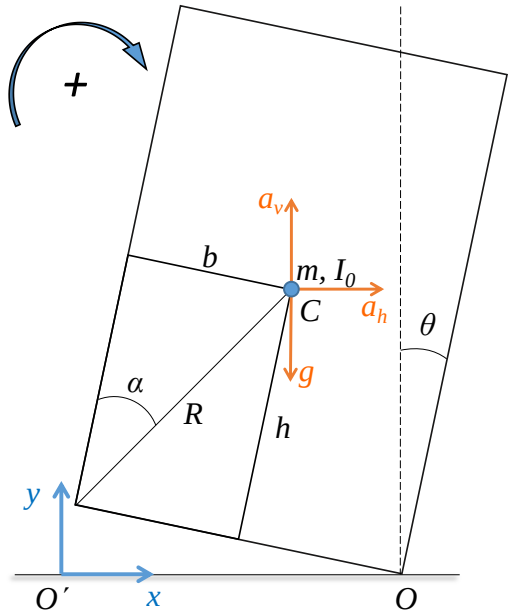

Figure 1: Rocking block sketch.

Symbol	Parameter
a_h	Horizontal seismic acceleration
a_v	Vertical seismic acceleration
b	Block half width
$b/h = tan(\alpha)$	Block aspect ratio
C	Centre of mass
g	Acceleration of gravity
h	Half block height
$I = mR^2/3$	Moment of inertia about C
$I_O = I+mR^2$	Moment of inertia about $O/O´$
O	Left corner indicator
O´	Right corner indicator
m	Block mass
R	Length of half diagonal
α	Slenderness (critical) angle
θ	Angle of rotation

Table 1. Rocking block parameters.

The rocking motion of a single block can be described by the variation of its angular position, θ, relative to the (horizontal) ground. A clockwise rotation is taken as the positive direction, therefore, the block is at positive angles when it rotates over its right corner O (Figure 1), and at negative angles when it rotates over its left corner, O'. The restoring force due to gravity is therefore negative or positive, respectively. The position of the block corners and center are calculated in a Cartesian system, the origin of which is at the lower left corner, O'.

In the present work, the motion of a single block or a two-block system is studied at first as free rocking motion, in which the blocks start from an initial non-zero angular position and rotate under the action of gravity. Subsequently, a forced excitation motion is considered, in which the ground undergoes a horizontal seismic acceleration, a_h (Figure 1). In this case, the calculations are made in the relative Cartesian system, so as the origin remains at point O' Vertical acceleration a_v can be also applied, by simply summing it along with g.

2.2 Theoretical model of a single block

The mathematical derivation is composed of two sections: the motion and the impact equations. Even though the equations of motion describe the behaviour of the block-ground system during uplift, impact equations are also important because they control the energy dissipation of the block.

2.2.1 Equations of motion

Since this is a dynamic problem, the Euler-Lagrange equation is usually used in multi-block studies to produce a second-order differential equation with respect to angle θ of the block [63]. Here it is also used for derivation of the single block motion equations.

$$\frac{d}{dt}\left(\frac{\partial T}{\partial \dot{\theta}_i}\right) - \frac{dT}{d\theta_i} = \frac{dW}{d\theta_i} \tag{1}$$

where T and dW is the kinetic and potential energy of the block, respectively, and i is the block number, which in this case is one. In order to establish the expressions of T and dW, the horizontal and vertical displacements (u_{CR}, v_{CR}) of the centre of mass are required (Figure 2). While rotation occurs around the lower right or left point, we can also define the displacements of the upper left/right corners that will be used later for two-blocks modelling:

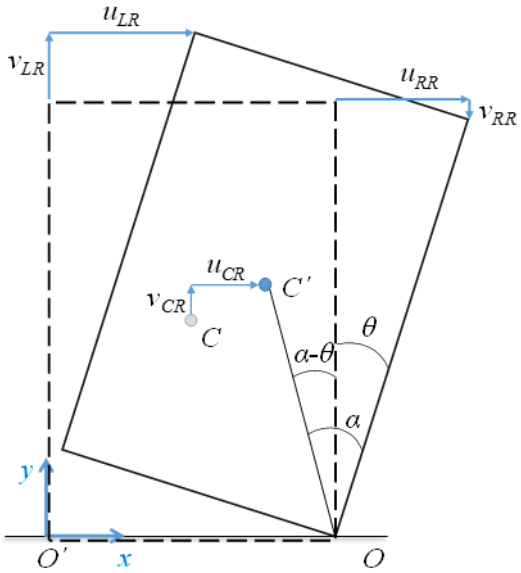

Figure 2: Definition of displacements.

$$u_{LR} = 2R[\sin(a) - \sin(a - \theta)] \quad (2)$$

$$v_{LR} = 2R[\cos(a - \theta) - \cos(a)] \quad (3)$$

$$u_{RR} = 2R\cos(a)\sin(\theta) \quad (4)$$

$$v_{RR} = 2R\cos(a)[\cos(\theta) - 1] \quad (5)$$

$$u_{CR} = \frac{u_{LR}}{2} \quad (6)$$

$$v_{CR} = \frac{v_{LR}}{2} \quad (7)$$

where the first subscript denotes the point of interest [upper left (L) or right (R) corner, or center (C)] and the second the left (L) or right (R) corner of rotation [e.g. Eq. (3) gives the vertical displacement of the upper left corner while the block rotates about the lower right corner]. Similarly, the corresponding expressions for rotation with respect to the lower left corner show some symmetry (though not exact) in respect to the rotation corner, and are given below:

$$u_{LL} = u_{RR} \quad (8)$$

$$v_{LL} = v_{RR} \quad (9)$$

$$u_{RL} = -2R[\sin(a) - \sin(\alpha + \theta)] \quad (10)$$

$$v_{RL} = 2R[\cos(a + \theta) - \cos(\alpha)] \quad (11)$$

$$u_{CL} = \frac{u_{RL}}{2}, \quad v_{CL} = \frac{v_{RL}}{2} \quad (12)$$

In order to reduce the number of equations and to obtain a single final equation for the motion of the block, regardless of the rotation corner, a binary indicator (C_R) has been introduced in the present work.

$$C_R = \begin{cases} 1, & rotation\ around\ right\ corner \\ 0, & rotation\ around\ left\ corner \end{cases} \quad (13)$$

In this way, the algorithm does not have to examine two separate cases, $\theta > 0$ and $\theta < 0$. This practice is adopted by other researchers as well, for a single rocking block [16, 18, 76]. This indicator is also used for the case of two blocks, thus achieving a significant gain in both simplicity and generality of the model. In the ensuing analyses the alternative (equivalent) definition $C_R = H(\theta)$ is employed, $H(\ )$ being the familiar Heaviside step function.

Thus, the general expression for the displacement of the center of mass becomes:

$$u_C = R[\sin(a) - \sin(\alpha - \theta)]C_R - R[\sin(\alpha) - \sin(\alpha + \theta)](1 - C_R) \quad (14)$$

$$v_C = R[\cos(a - \theta) - \cos(\alpha)]C_R + R[\cos(a + \theta) - \cos(\alpha)](1 - C_R) \quad (15)$$

The expressions for the kinetic and the potential energy of the block are accordingly:

$$T = \frac{1}{2} I_o \dot{\theta}^2 \tag{16}$$

$$\delta W = m[a_h u_c + (a_v + g) v_c] \tag{17}$$

By substitution of Eqs. (16) and (17) into (1) and after expanding on algebra, we finally get the general equation for the rocking motion of a single block:

$$\ddot{\theta} = \frac{m}{I_o} [a_h \frac{du_C}{d\theta} + (a_v + g) \frac{dv_C}{d\theta}] \tag{18}$$

where

$$\frac{du_C}{d\theta} = R[C_R \cos(a - \theta) + (1 - C_R) \cos(a + \theta)] \tag{19}$$

and

$$\frac{dv_C}{d\theta} = R[C_R \sin(a - \theta) - (1 - C_R) \sin(a + \theta)] \tag{20}$$

Note that the term $\frac{dT}{d\theta_i}$ is zero because the expression of *T* does not involve any θ_i terms.

2.2.2 Equations of impact

Under the assumption that the impact happens at a single point (corner) and lasts for an infinitesimal time interval, the angular impulse of the acting forces there can be neglected, and hence the angular momentum of the block about that corner does not change. In this way, the angular velocity of the block just after an impact can be found by applying the conservation of angular momentum, which is defined as

$$h = I\ \dot{\theta} + \vec{r} \times m \cdot \overrightarrow{V_C} \tag{21}$$

where $\vec{r}$ is the vector from a given point (here the rotation corner) to the centre of mass and $\overrightarrow{V_C}$ is the velocity vector of the centre of mass. Therefore, for an impact at left corner *O´* (Fig. 3), we have:

$$h_{o'}^{-} = h_{o'}^{+} \quad \rightarrow \quad [I + mR^2 \sin(\varphi)]\ \dot{\theta}^{-} = (I + mR^2) \dot{\theta}^{+} \tag{22}$$

where superscripts '–' and '+' denote conditions just before and just after the impact, respectively, and the angle φ is $\left(\frac{\pi}{2} - 2a\right)$, as shown in Figure 3.

Thus, the coefficient of restitution after an impact is defined as:

$$r = \frac{\dot{\theta}^+}{\dot{\theta}^-} = \frac{I+mR^2+\cos(2a)}{I+mR^2} = 1 - \frac{3}{2}\sin^2(a) \tag{23}$$

The above equation was first derived by Housner [8] who introduced the model of simple rocking motion of a single block. Using this simple expression, the angular velocity of the block just after an impact, $\dot{\theta}^+$, can be obtained from its previous value, $\dot{\theta}^-$, depending only on the aspect ratio of the block.

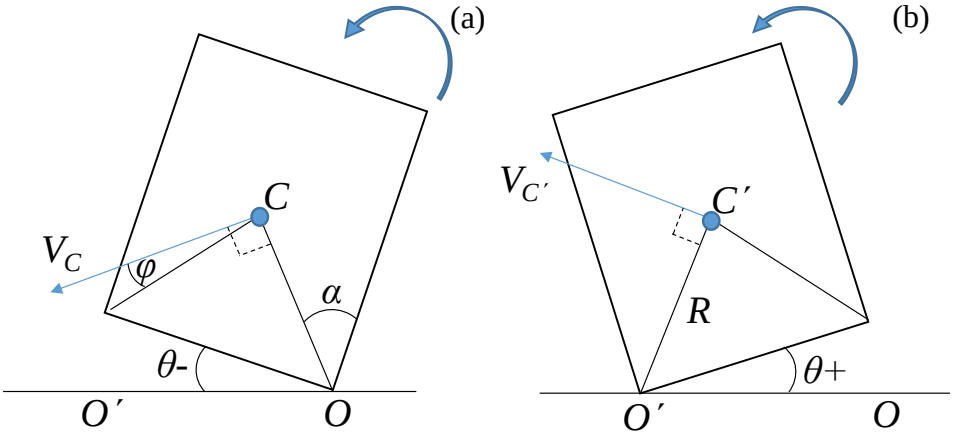

Figure 3: Rocking diagram: (a) before; and (b) after impact.

The value of the restitution coefficient is less than 1 (e.g. for $h/b = 2$ it becomes 0.7), therefore there is an amount of kinetic energy dissipated during the impact (Eq. 22). In real block systems, the dissipated energy during an impact is mainly transferred to the ground (through wave radiation [76]) but can also be spent in inelastic impact or friction mechanisms. However, the assumption of point impact and perfect rectangular geometry leads to an underestimation of r, the value of which may be significantly higher in practical systems [28, 62, 64]. This behaviour is considered in this study and will be discussed in later sections.

2.3 Theoretical model of two blocks

The advantage of the compact formulation with respect to piece-wise modelling is minor for the case of a single block (i.e. combine two equations to one), but becomes significant for an assembly of blocks. In the present work the binary indicators are properly introduced also for the case of two blocks, achieving a significant gain in both simplicity and generality of the model. In this case there are N = 8 configuration patterns, with a total number of 16 differential equations [78], whereas the present model uses only 2 equations. For a 3-DOF system of 3 stacked blocks there are 52 different equations in the piece-wise approach (26 configuration modes, [1], [73]), which would be reduced to only 3 by the present technique.

2.3.1 Equations of motion

The process of mathematical derivation for a system of two rigid blocks is similar to that for the single block. However, the equations that describe the blocks are now coupled, which requires a system to be solved simultaneously. To create such a system, the expressions of T and dW can be generalised for n blocks. Thus, Eq. (16) becomes

$$T = \frac{1}{2}\sum_{i=1}^{n} I_{oi}\left(\dot{\theta}_i\right)^2 + \frac{1}{2}\sum_{i=2}^{n} m_i[(\dot{u}_{Ti})^2 + (\dot{v}_{Ti})^2] \quad (24)$$

where u_{Ti} and v_{Ti} are the cumulative displacement at the centre of mass (Figure 4):

$$u_{Ti} = U_i + u_{Ci} \quad (25)$$

$$v_{Ti} = V_i + v_{Ci} \quad (26)$$

and U_i, V_i the displacement of block i caused by its supporting block (see also Figure 4).

$$U_i = (u_{Rj-1})C_{Rj} + (u_{Lj-1})\left(1 - C_{Rj}\right) + U_{i-1} \quad (27)$$

$$V_i = (v_{Rj-1})C_{Rj} + (v_{Lj-1})\left(1 - C_{Rj}\right) + V_{i-1} \quad (28)$$

and u_{Ci}, v_{Ci} the displacement of centre of mass due to the rotation of individual blocks (Eq. 14, 15).

Consequently, the first sum of kinetic energy expression (Eq. 24) is due to rotation whereas the second is due to translation of a block in respect to its rest point, as shown in Figure 4. For n = 2 blocks only U_2 and V_2 are computed, since $U_1 = V_1 = 0$.

Similarly, for n blocks equation (17) the potential energy becomes:

$$\delta W = \sum_{i}^{n} m_i[a_h u_{Ti} + (a_v + g)v_{Ti}] \quad (29)$$

By substituting the partial derivatives of Eqs. (24) and (29) into Eq. (1), a system of n simultaneous equations is created. For the present case the system consists of two equations, one being the derivatives with respect to θ_1 and the other to θ_2. The final system of differential equations describing the rocking motion of two blocks can be written as:

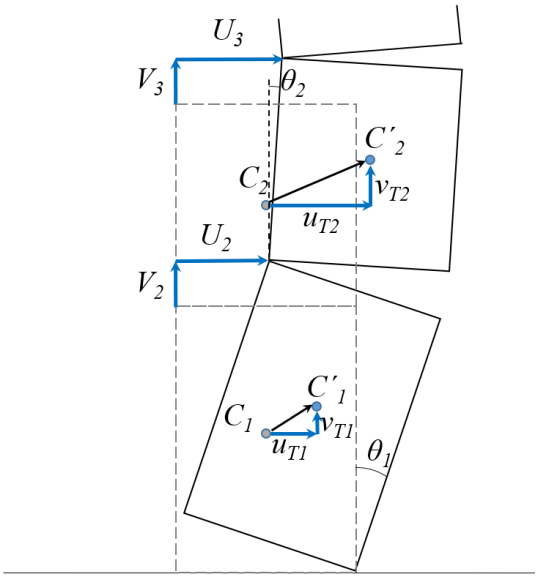

Figure 4: Rocking motion of two blocks.

$$\ddot{\theta}_1 = \left[\begin{matrix}-m_1\left(u_h\frac{du_{T1}}{d\theta_1}+(g+a_h)\frac{dv_{T1}}{d\theta_1}\right)-m_2\left(u_h\frac{du_{T2}}{d\theta_1}+(g+a_h)\frac{dv_{T2}}{d\theta_1}\right)\\ -2m_2R_2l\left(\dot{\theta}_2^2\cdot\sin(\gamma)\cdot C_{Z2}+\ddot{\theta}_2\cos(\gamma)\right)\end{matrix}\right]\cdot\frac{1}{I_{O1}+m_2.c}$$

$$\ddot{\theta}_2 = \left[\begin{matrix}-m_1\left(u_h\frac{du_{T1}}{d\theta_2}+(g+a_h)\frac{dv_{T1}}{d\theta_2}\right)-m_2\left(u_h\frac{du_{T2}}{d\theta_2}+(g+a_h)\frac{dv_{T2}}{d\theta_2}\right)\\ -2m_2R_2l\left(-\dot{\theta}_1^2\cdot\sin(\gamma)\cdot C_{Z2}+\ddot{\theta}_1\cos(\gamma)\right)\end{matrix}\right]\cdot\frac{1}{I_{O2}} \quad (30)$$

where

$$\frac{du_{T1}}{d\theta_1} = R_1[C_{R1}\cos(a_1-\theta_1)+(1-C_{R1})\cos(a_1+\theta_1)] \quad (31)$$

$$\frac{dv_{T1}}{d\theta_1} = R_1[C_{R1}\sin(a_1-\theta_1)-(1-C_{R1})\sin(a_1+\theta_1)] \quad (32)$$

$$\frac{du_{T2}}{d\theta_2} = R_2[C_{R2}\cos(a_2-\theta_2)+(1-C_{R2})\cos(a_2+\theta_2)] \quad (33)$$

$$\frac{dv_{T2}}{d\theta_2} = R_2[C_{R2}\sin(a_2-\theta_2)-(1-C_{R2})\sin(a_2+\theta_2)] \quad (34)$$

$$\frac{du_{T2}}{d\theta_1} = 2h_1\cos(\theta_1)(1-|C_{R1}-C_{R2}|)+2R_1|C_{R1}-C_{R2}|[\cos(\alpha_1-\theta_1)\,C_{R1}+\cos(\alpha_1-\theta_1)\,C_{R2}] \quad (35)$$

$$\frac{dv_{T2}}{d\theta_1} = -2h_1\sin(\theta_1)(1-|C_{R1}-C_{R2}|)+2R_1|C_{R1}-C_{R2}|[\sin(\alpha_1-\theta_1)\,C_{R1}-\sin(\alpha_1-\theta_1)\,C_{R2}] \quad (36)$$

$$\frac{du_{T1}}{d\theta_2} = \frac{dv_{T1}}{d\theta_2} = 0 \quad (37)$$

$$\gamma = a_2+|C_{R1}-C_{R2}|a_1+C_{Z2}(\theta_1-\theta_2) \quad (38)$$

$$b = R_1|C_{R1}-C_{R2}|+h_1(1-|C_{R1}-C_{R2}|) \quad (39)$$

$$c = 4R_1^2|C_{R1} - C_{R2}| + 4h_1^2(1 - |C_{R1} - C_{R2}|) \quad (40)$$

$$C_{Z2} = 2 \cdot C_{R2} - 1 = \begin{cases} 1, & rotation\ around\ right\ corner \\ -1, & rotation\ around\ left\ corner \end{cases} \quad (41)$$

in which C_{R1} and C_{R2} are the binary indicators of lower and upper block, respectively, as defined by Eq. (13).

2.3.2 Equations of impact

The derivation of the new angular velocities of the blocks after an impact ($\dot{\theta}_1^+, \dot{\theta}_2^+$), is based on the same principles as in Section 2.2.2. However, two critical differences can be noticed: (i) an impact may occur between two different sets of rigid bodies, ground-lower block or upper block-lower block; and (ii) the impacts for the latter occur at a variable rotation angle. Thus, a separate system of two equations need to be derived and solved for each impact case, in order to compute the new angular velocities from the conditions just before impact. To create such systems, the conservation of angular momentum was applied twice for each case and the final expressions represent the equivalent of Housner's equation for a two-block system.

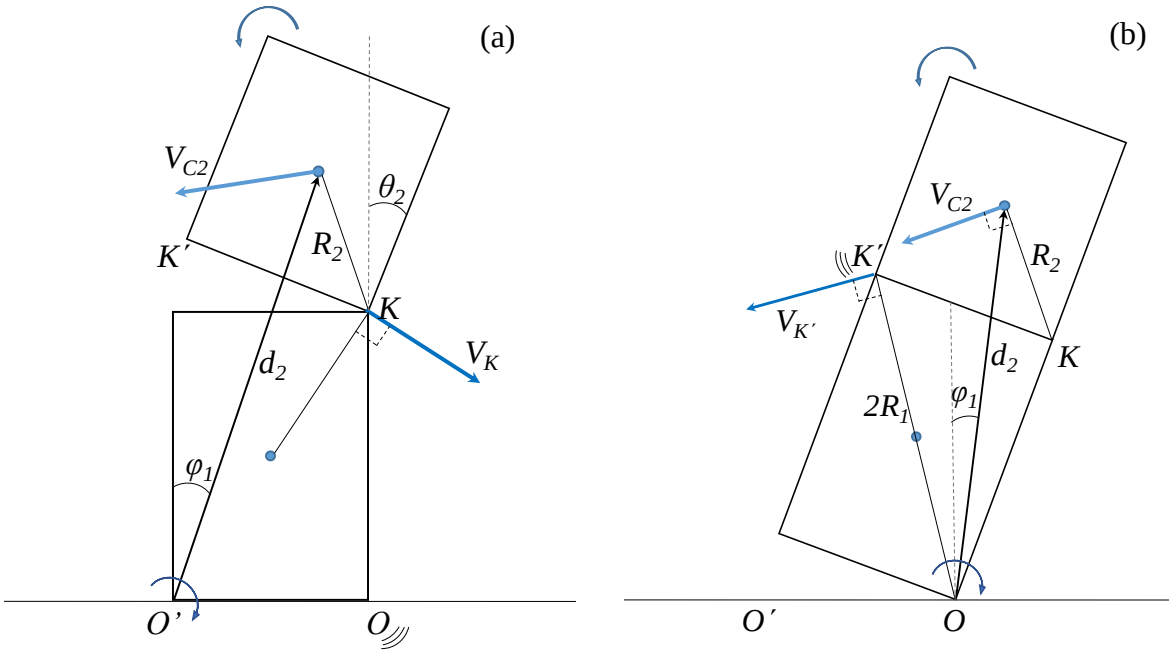

Figure 5: Two-block system impacts: (a) to the ground at the right corner *O*; and (b) between blocks at point *K′*.

Impact between lower block and the ground

Assuming that impact occurs at point *O* and the upper block rotating around *K*, as shown in Figure 5a, the two independent expressions that can be used are the conservation of angular momentum of the upper block alone with respect to *K*, and of the two-block system with respect to *O′*. For the lower block just before and just after the impact we have (Figure 5a):

$$h_{O'1}^- = I_1\dot{\theta}_1^- + m_1 R_1^2 \cos(2a_1)\,\dot{\theta}_1^- \quad (42)$$

$$h_{O'1}^+ = I_1\dot{\theta}_1^+ + m_1 R_1^2\,\dot{\theta}_1^+ \quad (43)$$

while for the upper block the expression remains the same:

$$h_{O'2} = I_2\dot{\theta}_2 + \ m_2\ \vec{d}_2 \times \vec{V}_{C2} \tag{44}$$

but the angular velocity and the velocity of the upper block centre of mass $\vec{V}_{C2}$ (Fig. 5) before and after the impact are different because the binary indicator C_{R1} changes after impact.

Also, for the upper block rotation with respect to *K* there is a single expression, in which again the velocities before and after the impact are different (Figure 5a).

$$h_{K2} = I_2\dot{\theta}_2 + m_2\ R_2^2\ \dot{\theta}_2 + \ m_2\ \vec{R}_2 \times \vec{V}_K \tag{45}$$

After deriving and analysing the terms of all the above expressions, the angular momentum conservation equations take the form of a set of two linear equations:

$$\begin{cases} h_{K2}^- = h_{K2}^+ \\ h_{O'1}^- + h_{O'2}^- = h_{O'1}^+ + h_{O'2}^+ \end{cases} \xrightarrow{yields} \begin{cases} A_1\dot{\theta}_1^+ + B_1\dot{\theta}_2^+ = C_1 \\ A_2\dot{\theta}_1^+ + B_2\dot{\theta}_2^+ = C_2 \end{cases} \tag{46}$$

where

$$A_1 = 2m_2R_2F^+ \tag{47}$$

$$B_1 = I_2 + m_2R_2^2 \tag{48}$$

$$C_1 = (I_2 + m_2R_2^2)\dot{\theta}_2^- \ + 2m_2R_2F^-\dot{\theta}_1^- \tag{49}$$

$$A_2 = I_1 + m_1R_1^2 + m_2d_1\big(E\cos(\varphi_1) - Z\sin(\varphi_1)\big) \tag{50}$$

$$B_2 = I_2 + m_2d_1(A\cos(\varphi_1) - B\sin(\varphi_1)) \tag{51}$$

$$C_2 = m_2d_1\big(C\dot{\theta}_1^-\cos(\varphi_1) + A\dot{\theta}_2^-\cos(\varphi_1) - D\dot{\theta}_1^-\sin(\varphi_1) - B\dot{\theta}_2^-\sin(\varphi_1)\big) + I_2\dot{\theta}_2^- + (I_1 + m_1R_1^2\cos(2a_1))\,\dot{\theta}_1^- \tag{52}$$

where

$$A = R_2[\cos(a_2 - \theta_2)C_{R2} + \cos(a_2 + \theta_2)(1 - C_{R2})] \tag{53}$$

$$B = R_2[\sin(a_2 - \theta_2)C_{R2} - \sin(a_2 + \theta_2)(1 - C_{R2})] \tag{54}$$

$$C = 2h_1(2C_{R1}C_{R2} + 1 - C_{R1} - C_{R2}) + 2R_1\cos(a_1)(C_{R1} + C_{R2} - 2C_{R1}C_{R2}) \tag{55}$$

$$D = 2R_1\sin(a_1)(C_{R1} - C_{R2}) \tag{56}$$

$$E = 2h_1[2(1 - C_{R1})C_{R2} + C_{R1} - C_{R2}] + 2R_1\cos(a_1)[(1 - C_{R1})(1 - 2C_{R2}) + C_{R2}] \tag{57}$$

$$Z = 2R_1\sin(a_1)[(1 - C_{R1}) - C_{R2}] \quad (58)$$

$$F^+ = h_1\cos(a_2 - C_{Z2}\theta_2)|C_{R1} - C_{R2}| + R_1\cos(a_1 + a_2 - C_{Z2}\theta_2)(1 - |C_{R1} - C_{R2}|) \quad (59)$$

$$F^- = h_1\cos(a_2 - C_{Z2}\theta_2)(1 - |C_{R1} - C_{R2}|) + R_1\cos(a_1 + a_2 - C_{Z2}\theta_2)|C_{R1} - C_{R2}| \quad (60)$$

$$\varphi_1 = \text{atan}\left(\frac{C_{Z1}b_2 + u_{c2}}{2h_1 + h_2 + v_{c2}}\right) \quad (61)$$

$$d_1 = \sqrt{(2h_1 + h_2 + v_{c2})^2 + (C_{Z1}b_2 + u_{c2})^2} \quad (62)$$

$$C_{Zi} = 2 \cdot C_{Ri} - 1 = \begin{cases} 1, & rotation\ around\ right\ corner \\ -1, & rotation\ around\ left\ corner \end{cases} \quad (63)$$

The same equations apply when the impact occurs at the other corner point, *O΄*, or when the upper box rotates about its left corner.

Impact between blocks

The governing equations for the second case were derived under a similar process and produced a similar linear system to Eq. 46. As shown in Figure 5b, the conservation of momentum for the upper block was applied about the point of impact (*K΄*), whereas for the system of blocks it was applied with respect to point *O*. Hence, the expressions of the various angular momentum terms are different (though similar to the previous). For the upper block, just before the impact at point K΄, the angular momentum is (Figure 5b):

$$h^-_{K'2} = I_2\dot{\theta}_2^- + m_2\, R_2^2\cos(2a_2)\dot{\theta}_2^- + \, m_2\, \vec{R}_2 \times \vec{V}_{K'} \quad (64)$$

and just after impact:

$$h^+_{K'2} = I_2\dot{\theta}_2^+ + m_2\, R_2^2\, \dot{\theta}_2^+ + \, m_2\, \vec{R}_2 \times \vec{V}_{K'} \quad (65)$$

Also, the expressions for blocks 1 and 2 with respect to point O are:

$$h_{O1} = I_1\dot{\theta}_1 + m_1\, R_1^2\, \dot{\theta}_1 \quad (66)$$

$$h_{O2} = I_2\dot{\theta}_2 + m_2\, \vec{d}_2 \times \vec{V}_{C2} \quad (67)$$

in which, again, the angular and linear velocities are different before and after impact.

By applying conservation of angular momentum in Eqs. (64) – (67), we end up with the same system as in Eq. (46) in which the coefficients are now as follows

$$A_1 = 2m_2R_2F^+ \quad (68)$$

$$B_1 = I_2 + m_2R_2^2 \quad (69)$$

$$C_1 = [I_2 + m_2R_2^2\cos(2a_2)]\dot{\theta}_2^- + 2m_2R_2F^-\dot{\theta}_1^- \quad (70)$$

$$A_2 = I_1 + m_1 R_1^2 + m_2 d_2 [E\cos(\varphi_2) - Z\sin(\varphi_2)] \quad (71)$$

$$B_2 = I_2 + m_2 d_2 [G\cos(\varphi_2) - H\sin(\varphi_2)] \quad (72)$$

$$C_2 = m_2 d_2 \left[C\dot{\theta}_1^- \cos(\varphi_2) + A\dot{\theta}_2^- \cos(\varphi_2) - D\dot{\theta}_1^- \sin(\varphi_2) - B\dot{\theta}_2^- \sin(\varphi_2)\right] + \\ + I_2\dot{\theta}_2^- + I_1\dot{\theta}_1^- + m_1 R_1^2 \dot{\theta}_1^- \quad (73)$$

where

$$A = R_2[\cos(a_2 - \theta_2)C_{R2} + \cos(a_2 + \theta_2)(1 - C_{R2})] \quad (74)$$

$$B = R_2[\sin(a_2 - \theta_2)C_{R2} - \sin(a_2 + \theta_2)(1 - C_{R2})] \quad (75)$$

$$C = 2h_1\cos(\theta_1)(2C_{R1}C_{R2} + 1 - C_{R1} - C_{R2}) + 2R_1[\cos(a_1 - \theta_1)C_{R1}(1 - C_{R2}) \\ + \cos(a_1 + \theta_1)C_{R2}(1 - C_{R1})] \quad (76)$$

$$D = -2h_1\sin(\theta_1)(2C_{R1}C_{R2} + 1 - C_{R1} - C_{R2}) + 2R_1[\sin(a_1 - \theta_1)C_{R1}(1 - C_{R2}) \\ - \sin(a_1 + \theta_1)C_{R2}(1 - C_{R1})] \quad (77)$$

$$E = [2h_1\cos(\theta_1)(2(1 - C_{R2})C_{R1} + C_{R2} - C_{R1})] + 2R_1[\cos(a_1 - \theta_1)C_{R1}C_{R2} \\ + \cos(a_1 + \theta_1)(1 - C_{R1})(1 - C_{R2})] \quad (78)$$

$$Z = [-2h_1\sin(\theta_1)(2(1 - C_{R2})CR_1 + C_{R2} - C_{R1})] + 2R_1[\sin(a_1 - \theta_1)C_{R1}C_{R2} \\ - \sin(a_1 + \theta_1)(1 - C_{R1})(1 - C_{R2})] \quad (79)$$

$$F^+ = R_1\cos(a_1 + a_2)(1 - |C_{R1} - C_{R2}|) + h_1\cos(a_2)|C_{R1} - C_{R2}| \quad (80)$$

$$F^- = F^+ \quad (81)$$

$$G = R_2[\cos(a_2 - \theta_2)(1 - C_{R2}) + \cos(a_2 + \theta_2)C_{R2}] \quad (82)$$

$$H = R_2[\sin(a_2 - \theta_2)(1 - C_{R2}) - \sin(a_2 + \theta_2)C_{R2}] \quad (83)$$

$$\varphi_2 = \theta_1 - \text{atan}\left(\frac{C_{Z1}b_2}{2h_1 + h_2}\right) \quad (84)$$

$$d_2 = \sqrt{(2h_1 + h_2)^2 + (b_2)^2} \quad (85)$$

The same equations apply when the impact is at point *K*, or if the lower block rotates about *O'* where only the values of the binary indicators C_{R1} and C_{R2} are adjusted according to Eq. (13).

2.4 Numerical analysis

An additional advantage of the present formulation is that it does not make use of conditions and checks to identify uplift or detachment of the blocks from each other. This can be accomplished as follows: At the start of simulation the block is considered to rotate around its right corner (Fig. 1), though being at zero angle $\theta_1 = 0$. Then, integration of Eq. (18) for one time-step results to a positive or negative acceleration and rotation angle, depending on the excitation amplitude (even at zero excitation there is still the action of gravity). If the external excitation is strong enough to achieve uplift, the integration results in a positive angle, $\theta_1 > 0$ (Fig. 1) that continues to increase in the ensuing time steps. In the opposite case (or if only gravity acts), the result would be a negative angle, $\theta_1 < 0$, which would activate the impact equations leading to the rebound velocities around the opposite corner. As long as the excitation

cannot induce uplift of the block, this procedure is repeated until a termination criterion is activated (see discussion below). In such non-uplift conditions, the computed rebound values of the block angular acceleration from Eq. (18) are almost zero (below 10^{-10}), and hence the block remains effectively at rest.

Similar is the treatment of impact and detachment of the two blocks from each other, based on the integration of Eqs. (30). This method is more computationally expensive but only during non-uplift/detachment phases and not when the blocks are rotating. Yet, the benefits stemming from the simplicity and generality of the algorithm are significant, especially for the two-block system, where the number of possible uplift/detachment configurations becomes much higher (16, compared to 2 for a single block).

The non-linear, second-order differential equation (18) for a single block, or the system of Eqs. (30) for the two-blocks do not have an analytic solution and hence must be solved numerically. Linearisation of these equations for small rocking angles is possible, but the resulting solutions were found to deviate considerably from the rigorous results in certain cases [36]. In order to be numerically solved, the second-order governing differential equation is decomposed into a pair of two first-order differential equations using the familiar state-space form:

$$\frac{d\theta}{dt} = \dot{\theta} = \omega \tag{86}$$

$$\frac{d\omega}{dt} = \ddot{\theta} \tag{87}$$

where $\ddot{\theta}$ is taken from Eqs. (18) or (30), and ω is an auxiliary variable equal to angular velocity.

The system of the above equations was solved using a 4th order Runge-Kutta scheme, after it was proven to converge faster than the 1st order Euler method and a 2nd order Runge-Kutta. To do that, an 'accurate' solution was first calculated, using a very small reference time step [$\Delta t = 10^{-6}$ *s*, corresponding to a dimensionless time step, $(\Delta t \cdot p) = 1.05 \cdot 10^{-5}$, where p is the frequency parameter given in Eq. (90)],with which all methods produced the same results for the free rocking of a block with aspect ratio 1:2, released from an initial angle of +10 degrees. Then, the capability of each method to reproduce this rocking performance was tested using progressively increased time steps. An example of this procedure is shown in Figure 6a for a time step of 5×10^{-4} *s*. For this time step, the Euler method gives quite different results, whereas RK4 follows the correct curve at least for the first impacts (when $\theta = 0$).

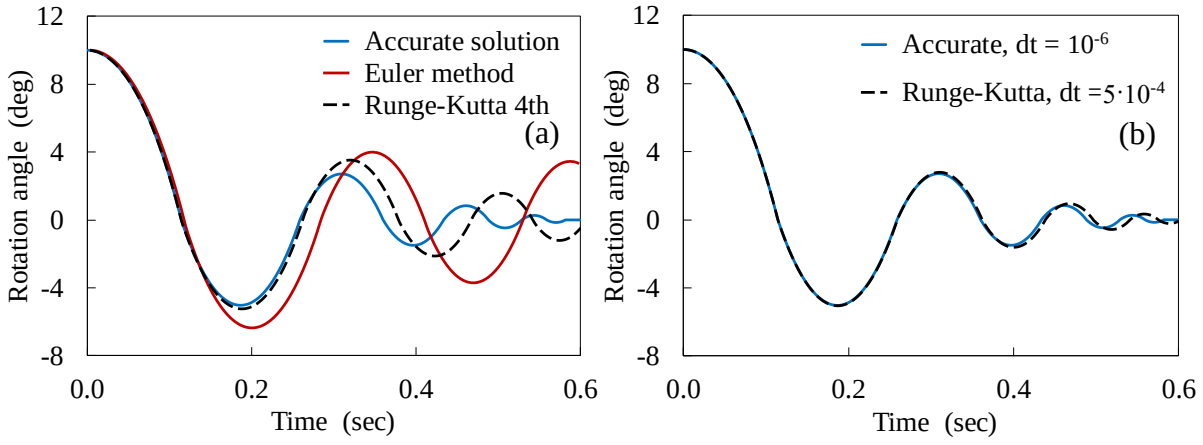

Figure 6: Comparison of results accuracy using different: (a) numerical methods; and (b) integration time step.

The time step independence was then investigated and the results of RK4 method were found to be almost identical with the reference solution using a time step of 5×10^{-4} s, as shown in Figure 6b. Consequently, a five-times smaller time step of 10^{-4} s [dimensionless time step ($\Delta t \cdot p$) of about 10^{-3}] is considered adequate to produce always sufficiently accurate numerical results, and it is employed throughout this study. Additional discussion on convergence issues is provided later in this paper.

For the two-block problem, four coupled ordinary differential equations are solved simultaneously by the RK4 method, which was programmed in the computer algorithm for that purpose. In addition to the numerical integration, the developed computer code checks if the impact conditions are met at each time step (impact with the ground or between the blocks). In such case, it computes the restitution coefficient from Eq. (23) for the single block problem or calculates the coefficients and solves the linear system in Eq. (46) for the two-block problem, to establish the angular velocity of the block(s) after an impact. This is then taken as the new initial condition to continue the integration of the rocking motion equations.

It is worth mentioning that without any special condition, the graphs of Figure 6 will continue to oscillate around the x-axis. When a minimum amplitude is reached, the oscillations will persist due to the computational accuracy of the computer. However, a block undergoing free oscillations will stop at a finite time, albeit after an infinite number of impacts [33]. A reasonable way to simulate the block at rest would be to introduce a termination criterion which stops the computations when the block impacts with the ground with a sufficiently small angular velocity, so as $|\dot{\theta}|/p < \varepsilon$, where ε is a pertinent tolerance parameter and p is the normalization parameter given by Eq. (90). This criterion was tested in various cases and found to perform satisfactorily, namely to terminate the algorithm when the oscillations of the block become minor. It must be noted that the criterion is applied only in the free rocking case of a single block, whereas in forced rocking or in two-block systems an overturning check is used in conjunction with a maximum integration time limit.

The CPU time required for a complete evaluation of a rocking case by the developed software is very small, and for the present studies it takes a few seconds on a desktop computer.

2.5 Experimental set-up

Free rocking motion after initial displacement

To confirm the reliability and accuracy of the theoretical expressions and numerical results, a number of experiments were conducted using steel rectangular blocks of different sizes (Figures 7 & 8). Using the camera of an iPhone 6 and the application SloPro, which provided slow motion recordings of up to 100 frames per second, the free rocking motion of the blocks was recorded after an initial angular displacement. Thereafter, the angles at which the angular velocity becomes zero (namely at the top oscillation points of the block, where the accuracy of measurement maximizes) were tabulated, along with the corresponding time instant at which they occurred, using a virtual on-screen protractor, as shown in Figure 7.

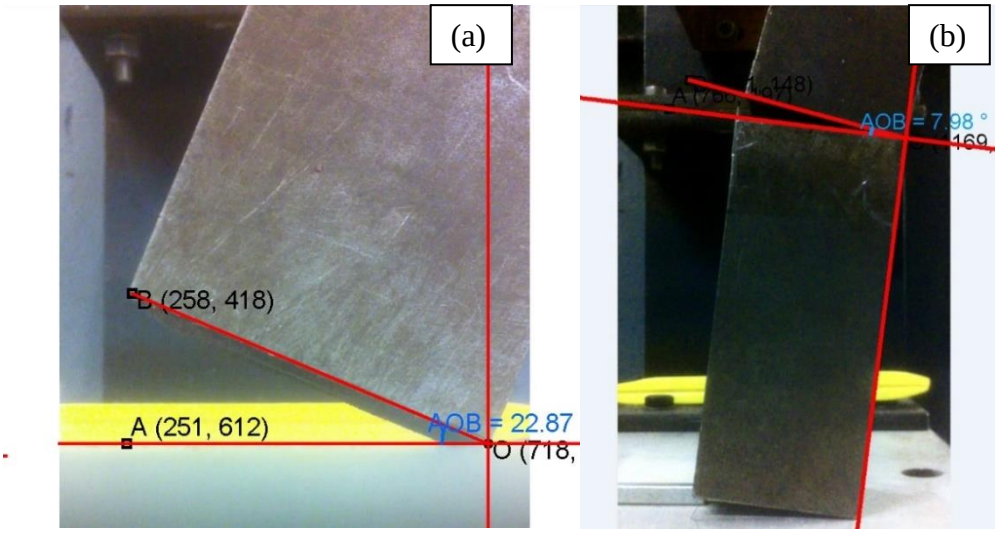

Figure 7: Snapshots from experimental recordings of: (a) single; and (b) double block free rocking and on-screen protractor software (in red).

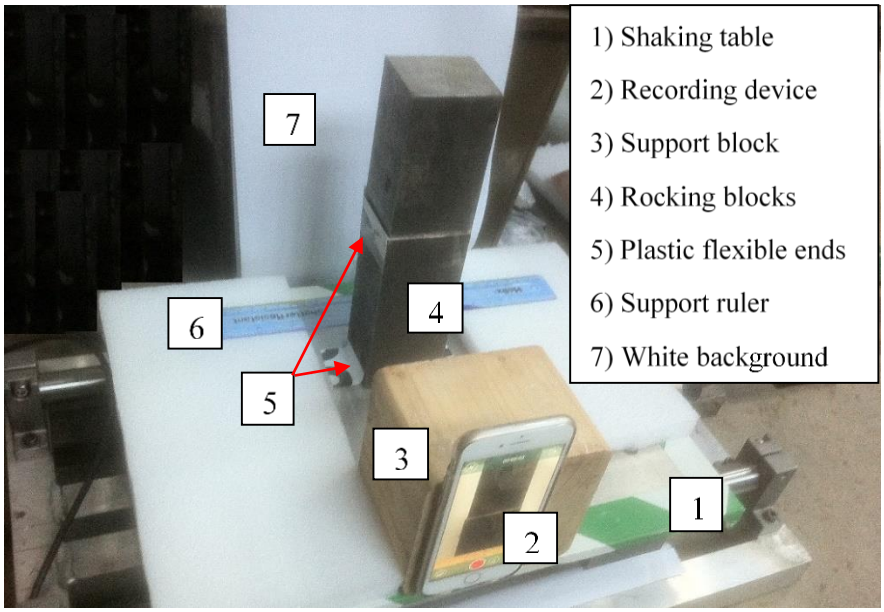

Figure 8: Shaking table apparatus.

In an attempt to approximate as much as possible, the ideal conditions of the theoretical analysis, the experiments were conducted under specifications that verged on the initial assumptions. Thus, to maximise the validity of the experiments and minimise the unknowns of the environment, the following measures were taken:

a) The horizontal levelling of the experimental base surface was tested.
b) The ground surface was steel to best approximate a rigid base.
c) Each block was selected for having sharp edges to ensure point impact.
d) Sliding was prevented using aluminium oxide sandpaper on the surfaces of contact.
e) The camera lens was placed on the same level as the examined surface of the block.
f) A small prop which held the block at an initial angle was instantaneously removed to initiate rocking. To ensure that no energy was given to the system, the initial angle of

each block was its critical angle which was calculated by a protractor. In that way, if a small amount of energy was given to the system as the prop was removed, the block would tip over.

g) To estimate the error margin, each experiment was repeated three times. Thus, three separate sets of measurements were extracted.

Forced rocking motion

In addition to the free rocking experiments, the forced rocking motion of single and two-block systems caused by horizontal vibrations is also investigated in the laboratory. To create such external excitation, the University of Bristol small shaking table at EQUALS laboratory was used for the tests (Figure 8). Several forced rocking videos were recorded under sinusoidal vibrations with amplitudes of 1.5, 3, 4 and 5*mm*. Each time, the frequency was gradually increased up to a point where the angular displacements could be easily measured. The previously stated measures for single block experiments were also taken for the two-block system. Additionally, eight extra measures had to be taken for the new configuration to ensure the credibility of the recorded data, as shown in Figure 8:

a) The shaking table was fixed to the ground using bolt connections.
b) The recording device was fixed to the shaking table to measure the displacements of the blocks relative to the table.
c) A wooden block was used to support the smart-phone so that the camera lay on the same plane as the block side of interest.
d) Any additional shaking of the supporting block and the recording device relative to the table was minimised.
e) To avoid sliding the use of sand paper was not enough. Thus, small pieces of flexible plastic were also placed at block sides perpendicular to the areas of contact.
f) A ruler made from hard plastic was fixed on the table to prevent blocks from sliding in the *z*-axis due to the impacts.
g) A white background was placed behind the blocks to increase the contrast with the darker blocks and facilitate the angle measurements on the recordings.
h) The two blocks had the same area of contact

3 Results

3.1 Single block analysis

3.1.1 Rocking response

The developed computer code provides plots with the variation of $\theta, \dot{\theta}, \ddot{\theta}$, a_h and a_v, as well as an animation of the simulated motion of the block. Such plots are indicatively drawn in Figure 9 for a free rocking block. It can be seen that the block follows a periodic (though not sinusoidal) pattern where both the amplitude and the period are damped. Evidently, the function θ cannot be characterised by the basic trigonometric functions, since its derivative, $\dot{\theta}$, develops sharp edges at impacts. Furthermore, the angular acceleration follows the damped oscillation of the angle and develops discontinuities at impacts (Figure 9c).

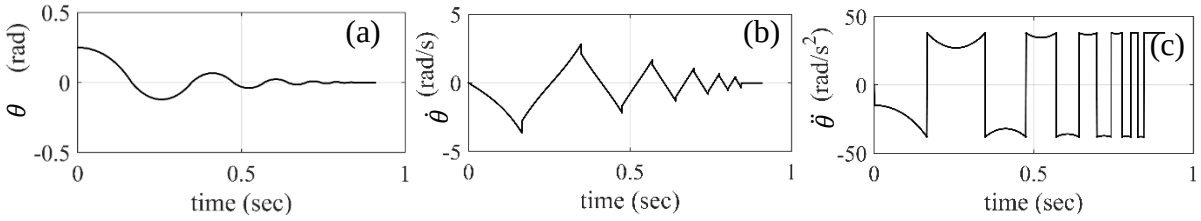

Figure 9: Indicative variation of: (a) angle; (b) angular velocity; and (c) acceleration of a free rocking block for $\theta(0)=25^o$ rad (Housner impact model).

On the other hand, when external sinusoidal accelerations, a_h and a_v, are introduced (ground excitation) the variation of $\theta, \dot{\theta}, \ddot{\theta}$ becomes more complex and sometimes chaotic-like, as shown in Figure 10. Yet, the sharp edges of $\dot{\theta}$ at impact are still visible, causing the discontinuities in the angular acceleration.

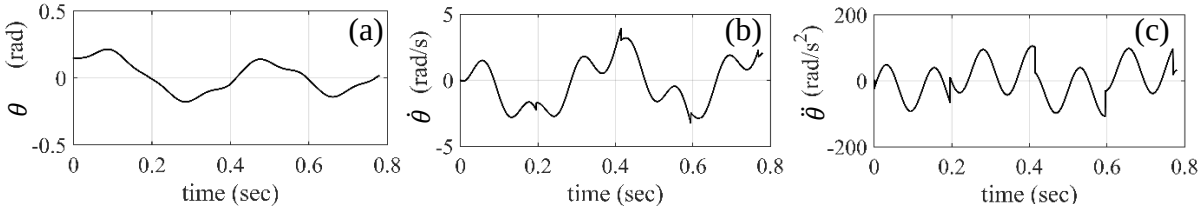

Figure 10: Indicative chaotic-like responses of: (a) angle; (b) angular velocity; and (c) acceleration for a single block under sinusoidal acceleration input (Housner impact model).

3.1.2 Experimental and numerical results

The dimensions and mass of each block as measured in the laboratory are tabulated below.

Table 2. Block properties

	Dimensions (*mm*): height x length x depth	Mass (*kg*)	Aspect ratio (*b/h*)	Slenderness angle α (deg)
Block 1	120 x 29 x 45	1.3	0.2417	13.6
Block 2	135 x 60 x 50	2.95	0.4445	24
Block 3	235 x 60 x 50	5.3	0.2553	14.3
Block 4	100 x 60 x 50	2.3	0.6	31

Since this is a 2-D problem, the dimension perpendicular to the plane of rotation is not affecting the motion of the block. Thus, the depth was used only for the mass calculation.

Figure 11 includes numerical and experimental results for the free rocking of Block 2, starting from angular position of +22º. Three different sets of measurements are included in this figure to demonstrate and estimate the experimental errors. This will be discussed in section 4.2, along with the comparison between measurements and numerical results.

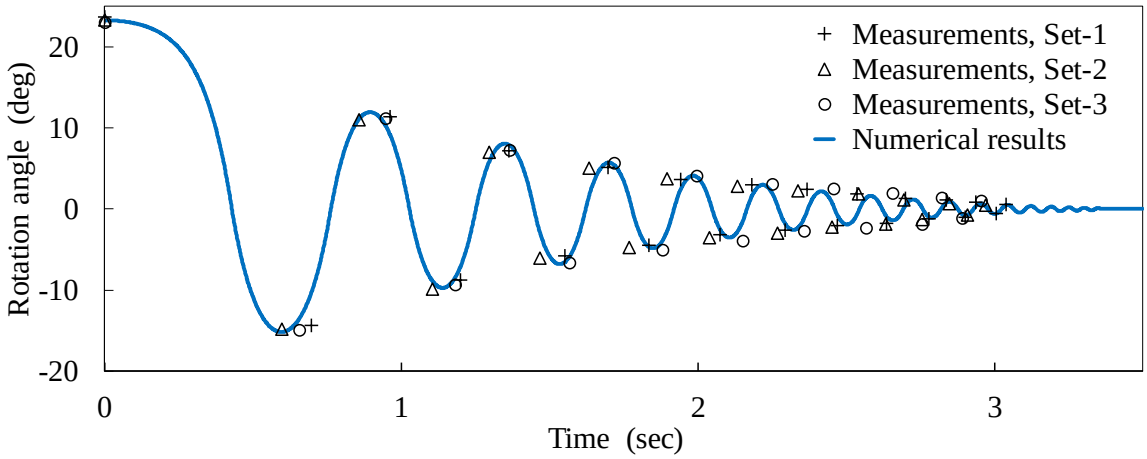

Figure 11: Comparison of free rocking experimental and numerical results for Block 2 with initial displacement of +22°.

Similar experiments were performed under the same assumptions for blocks 1 and 3 (Table 2) and the results are shown in Figure 12. The behaviour of the rocking blocks is similar, but the decay rate of the amplitude and period differs, although they have similar aspect ratio and initial angular position, because it depends on the eigen-frequency of their free rocking motion (frequency parameter, p in Equation 90). The latter is almost double for the smaller block 1, and hence it exhibits about half oscillation period and double decay rate (Fig. 12a). Again, three sets of measurements were taken for Blocks 1 and 3. However, for the error estimation of the rotation angle measurements in section 4.2, the only data sets used are the ones shown in Figure 11 since the highest discrepancy in the measurements occurred for Block 2.

Concerning forced rocking conditions, the experimental measurements of Figure 13 are for Block 2 subjected to an external vibration with frequency of 5 *Hz* and amplitude of 3 *mm*, after it has reached a periodic-like motion. In practice, the block performs a chaotic-like motion until it reaches a state-state like response, as it was also confirmed by the numerical results of the time interval from 0 to 3 seconds in Figure 13.

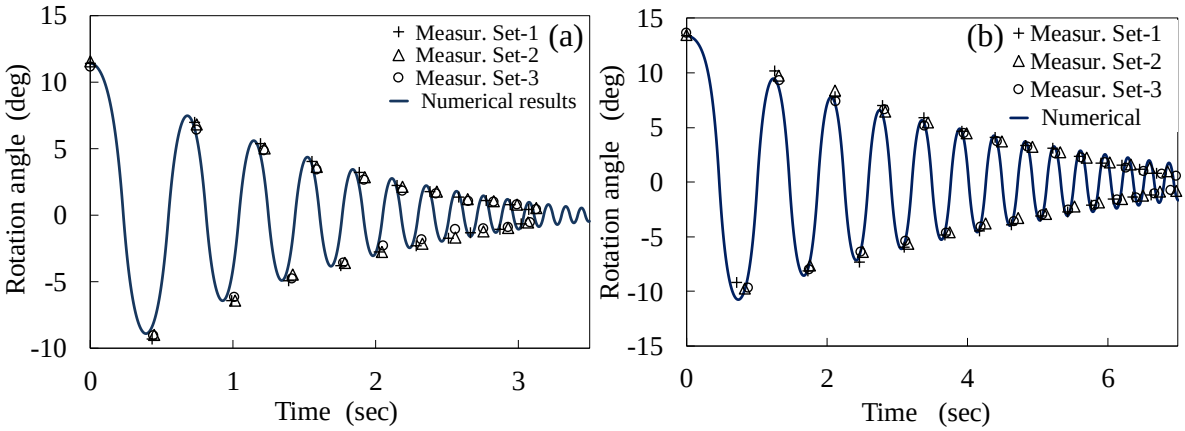

Figure 12: Comparison between experimental and numerical results for: (a) block 1; and (b) block 3 with initial displacements of +11.5° and +13°, respectively.

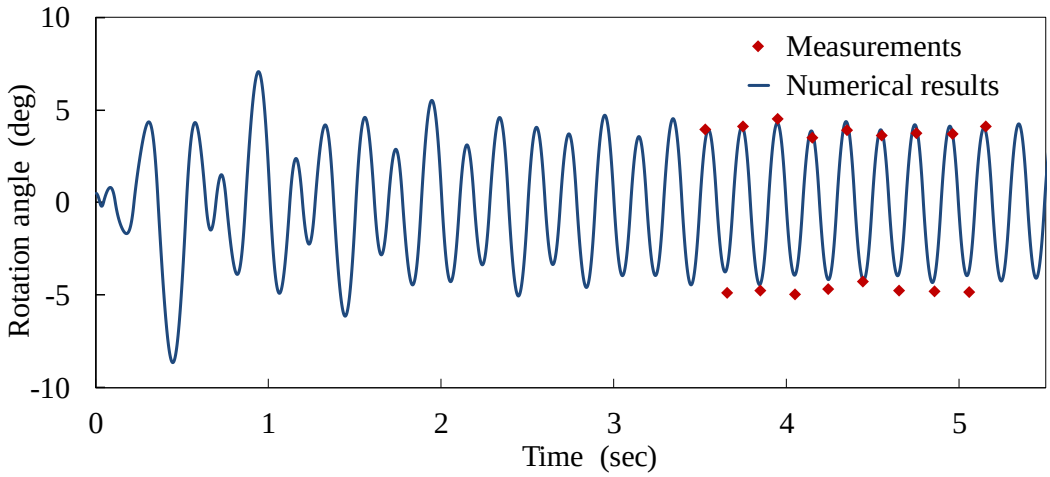

Figure 13: Experimental and numerical results for Block 2 under sinusoidal excitation of 5 *Hz* and 3*mm* amplitude.

3.2 Two-block system analysis

3.2.1 Numerical rocking response

To verify that the code was self-consistent, various symmetry tests were performed, at first for single block free rocking and then for the more complex combined motion of two blocks. In the latter, the angle variation with time was recorded after an initial angular displacement of the blocks and repeated for symmetric initial position of the blocks, as shown in Figure 14a. For this particular case the blocks start with opposite initial angles and perform chaotic-like rocking motion with impacts to the ground and among them (intersection points), for about 0.55 seconds. Then, they lock and behave as a single block.

As evident from Figure 14b, the angle variation curves of the second test with opposite initial displacement of the blocks were perfectly symmetric, and this is also valid for the precise quantitatively results, thus adding confidence as to the correctness of both the derived mathematical model and its incorporation into the computer algorithm.

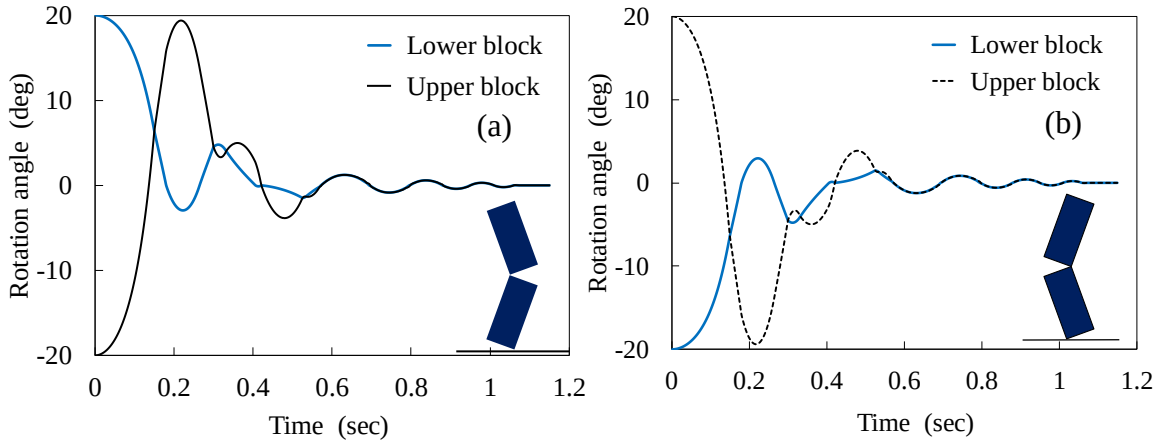

Figure 14: Numerical model self-consistency test for opposite block configurations. upper/lower block angle: (a) +/- 20º; (b), upper/lower block angle: -/+ 20º.

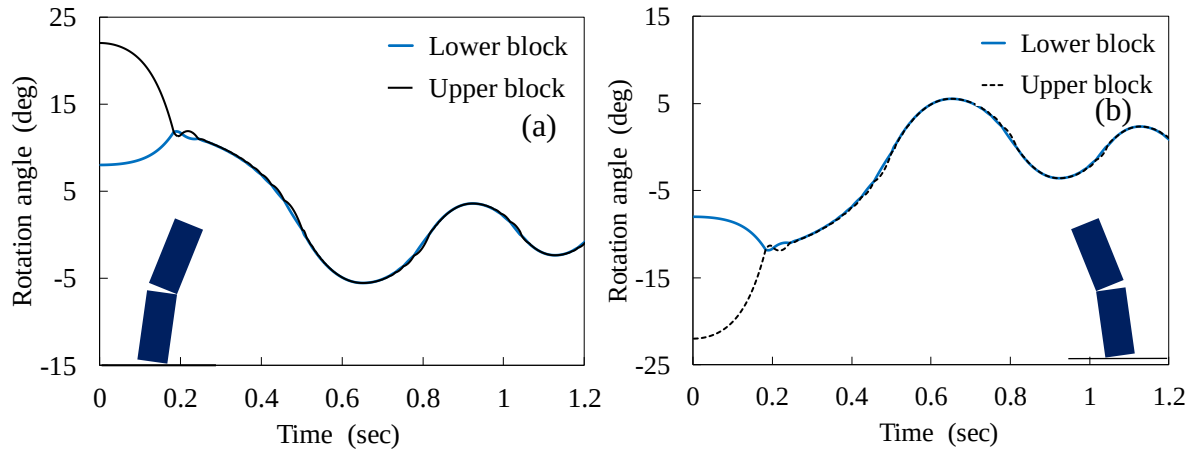

Figure 15: Model self-consistency test for two anti-symmetric block configurations: (a) upper/lower block angle: +23º /+8º; (b) upper/lower block angle: –23º /–8º.

An additional check of the correctness and accuracy of numerical results was carried out using a configuration of blocks with the same direction of initial angular displacement (Fig. 15). In this case, the two blocks rotate in opposite directions until they collide with each other. This first impact is followed by a few minor rocking oscillations of the upper block until the two blocks stick together and continue to rock as a single body. The resulting rocking curves for anti-symmetric initial position of blocks are, again, as expected (Fig. 15).

3.2.2 Experimental and numerical results

In Figure 16a, two sets of measurements are compared with the numerical results of the angle variation obtained from the algorithm for Blocks 1 (lower) and 4 (upper). In Figure 16b the restitution coefficients in the numerical model were adjusted to match the numerical results with the measurements, as will be discussed in Section 4. Note that up to 0.6 seconds the extracted measurements are denser to get a better representation of the impacts that occur before the blocks lock.

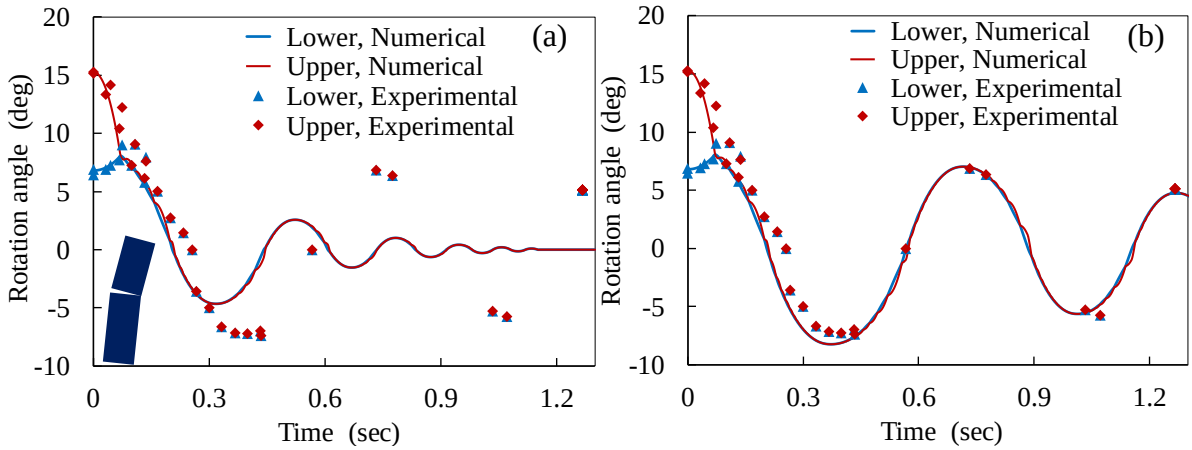

Figure 16: Comparison of two-block free rocking measurements and numerical results obtained by: (a) the present impact model, and (b) adjusted restitution coefficients. Upper/lower block angle: +15º / +7º.

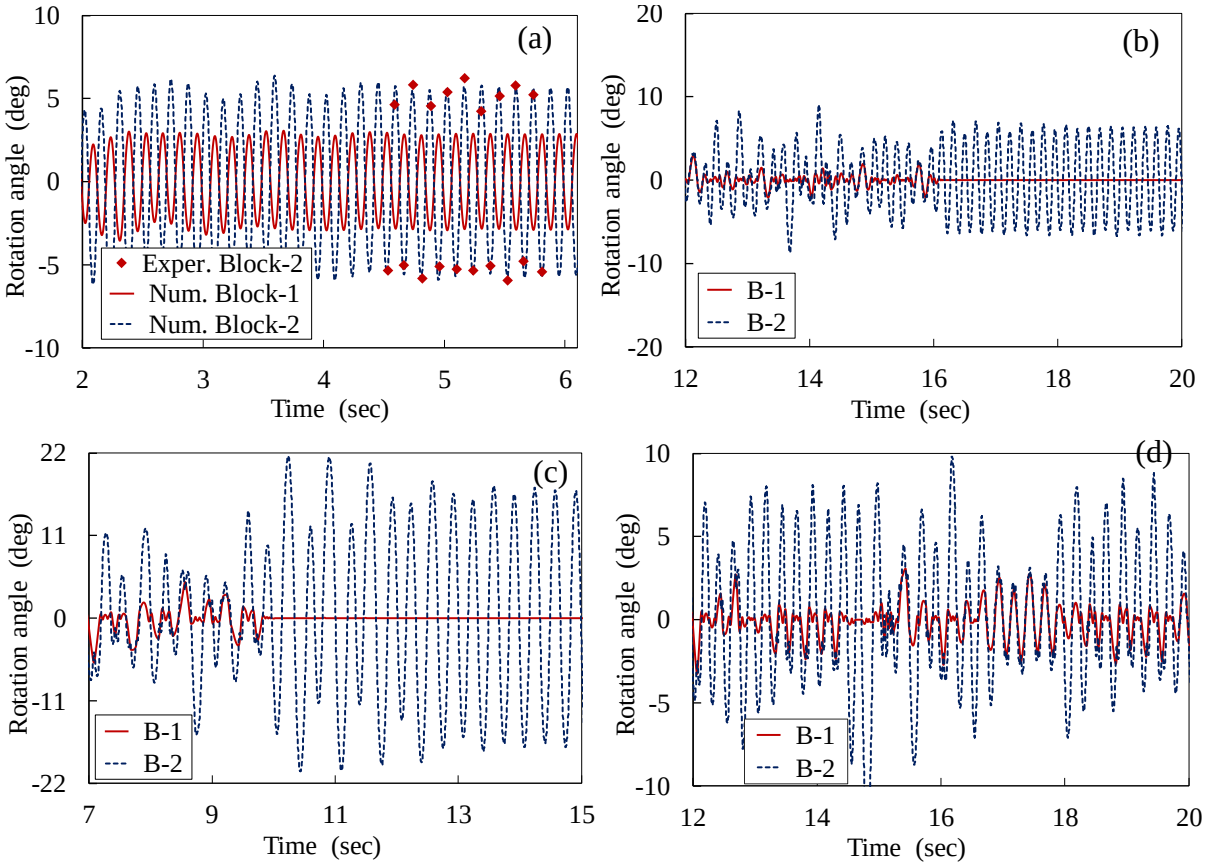

Figure 17: Various motives of two-block rocking forced by external excitations. Vibration amplitude (*mm*) / frequency (*Hz*): (a) 7/3, (c) 5.5/3 (c), 3/5, (d) 4/3.

Using the same block configuration as in Figure 16, various forced rocking experiments and numerical simulations were performed for different combinations of amplitude and frequency of a horizontal sinusoidal excitation. Some indicative results are shown in Figure 17, revealing the great complexity and diversity of the two-block system response to external acceleration forces, as will be discussed in the next section. This behaviour makes the performance of measurements with desirable accuracy difficult. A set of experimental data for the upper block only, obtained for relatively periodic behaviour of both blocks is shown in Fig. 17a.

3.3 Overturning study

Single block study

The numerical algorithm was applied to simulate the overturning behaviour of a single rigid block, subjected to a single sinusoidal acceleration pulse in the horizontal direction:

$$a_h = a_g \sin(\omega_g t) \tag{89}$$

where a_g is the amplitude and ω_g the angular frequency of the pulse. The resulting overturning maps are presented in normalised form in Figure 18, where the frequency parameter, p, is:

$$p = \sqrt{\frac{3g}{4R}} \tag{90}$$

The maps of Fig. 18 are created on a 10^2 x 10^2 grid in (a_g/g a, ω_g/p) space that corresponds

to 10^4 evaluations of the computer algorithm. In each evaluation, the equation of motion is integrated up to a dimensionless time ($p\ t_{max}$) = 10^2 and overturning is detected for $\theta = \pi/2$. Fig. 18a is obtained using the adjusted restitution coefficient r = 0.85 for α = 20º, whereas Fig. 18b shows the same map obtained by the Housner's geometric restitution coefficient in Eq. (23) (r = 0.82). The maps are divided into four regions: (i) region 0 where the block remains at rest; (ii) region 1 that represents stable rocking (no overturning); (iii) region 2 where the block overturns after one impact; and (iv) region 3 where the block overturns without impact. These regions are clearly bounded in the map, and region 3 is practically the same for both restitution models. However, region 2 is much restricted in the case of Housner's coefficient of restitution, which therefore predicts a larger stable region than that with the corrected and more realistic restitution. These results are compatible with those originally presented by Zhang & Makris [16] and Dimitrakopoulos & De Jong [29].

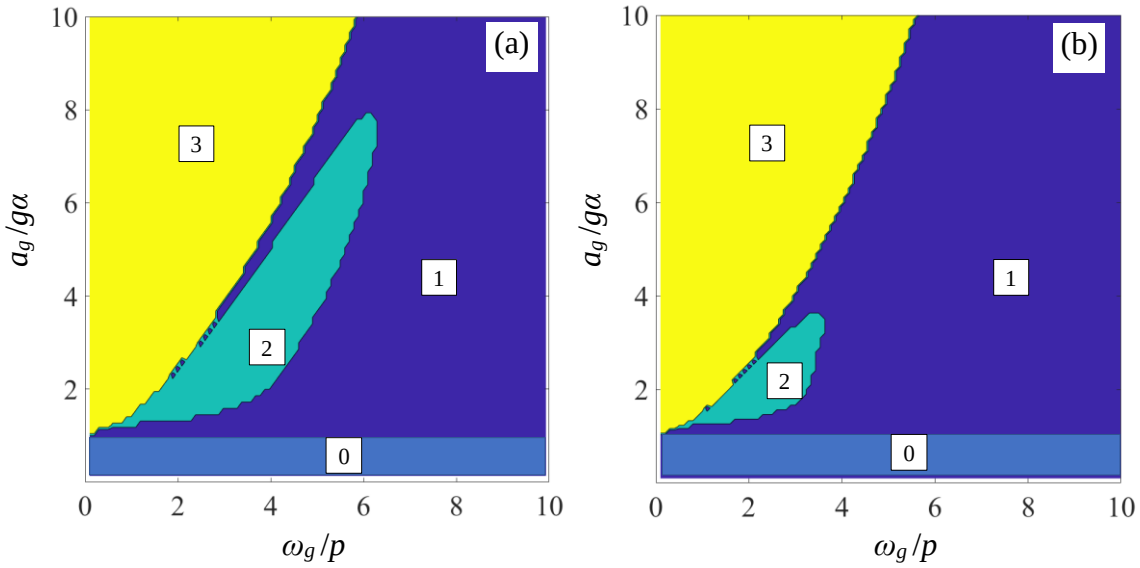

Figure 18: Overturning maps for a rocking block (α = 20º), subjected to single sinus pulse using: (a) the corrected restitution coefficient (r = 0.85) and (b) Housner's restitution coefficient from Eq. (23), (r = 0.82)

Two blocks study

The overturning study is extended to map the behaviour of double-block systems of the same aspect ratio (1:2 each). The normalisation was done assuming that the system was a single block with aspect ratio 1:4 (α = 14 degrees).

Figure 19a shows the produced map using the same restitution coefficient for all impacts of both blocks, equal to 0.85 [29]. However, this is a simplistic approximation. The map obtained in Figure 19b was produced from the analytical model (conservation of angular momentum) and the solution of system (46), for both impacts (lower block to ground, and between blocks). The regions of both maps are as follows:

0: No uplift

1a: Rocking motion as a single block

1b: Rocking of 2nd block on top of the 1st (relative angle > 0.01 rad = 0.57 degrees).

2: Overturning after one impact to the ground (usually, the 2nd block overturns first)

3: Overturning without impact to the ground (usually, the 1st block first, followed by the 2nd)

The application of constant coefficient of restitution for both blocks (Fig. 19a) provides well defined regions. However, the interface between regions 2 and 3 does not follow the exponential-like trend produced for the single block case of Figure 18. Furthermore, the regions where there is overturning (2, 3) appear to cover a large proportion of the map (> 50%) which implies that the double block system is more prone to overturn than to maintain a rocking motion when subject to a sinusoidal pulse.

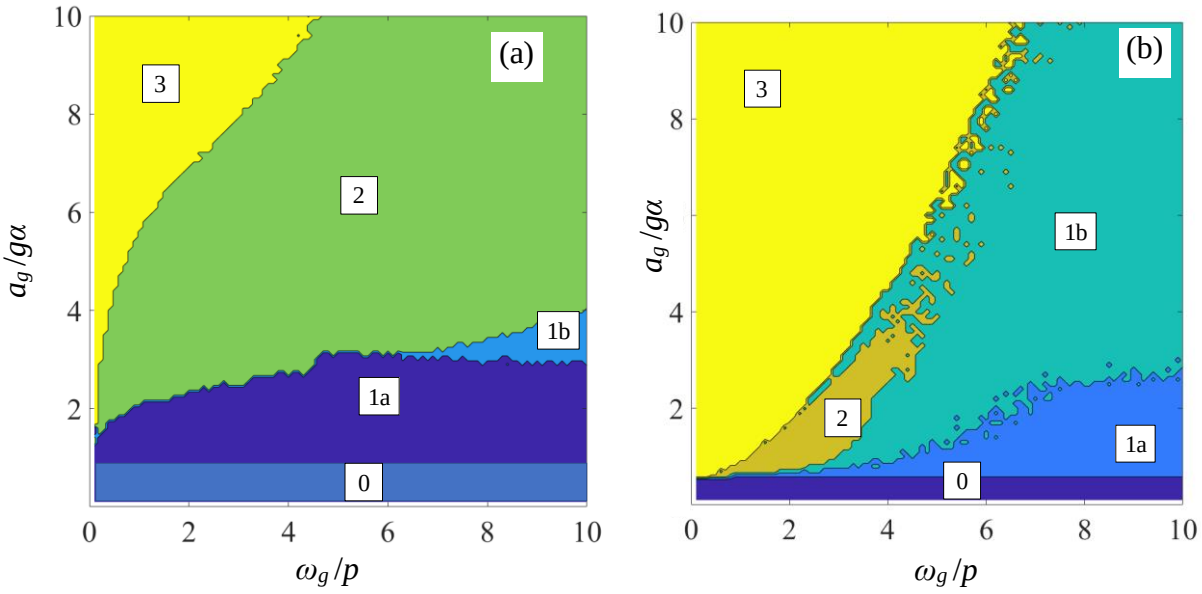

Figure 19: Overturning maps for a system of two blocks subjected to singe sinusoidal pulse using the corrected coefficients of restitution: (a) and the ones obtained from the solution of the impact model in Eq. (46b).

By replacing the pre-defined constant restitution with the solution of the conservation of momentum system of Eqs. (46), the resulting regions appear to produce a profile that resembles the single block cases, where the interface between the unstable regions appears to increase exponentially. However, an interface scattering effect appears to take place which could be attributed to the sensitivity of the system to the initial conditions, in the sense of deterministic chaos. As more blocks are introduced, a chaotic pattern emerges in the overturning maps of the two blocks. Two detailed magnifications of the scattering between regions 2 and 1b of Figure 19b are shown in Figure 20. Each magnification is the product of a separate simulation run with a grid composed of 100 x 100 cells, thus achieving a resolution increase of $x10^1$, $x10^2$, $x10^3$ in Figures 20b, 20c and 20d, respectively. Evidently, this chaotic pattern seems to be fractal in nature (scale invariance patterns are evident in Figs 19c and 19d) and it is also reminiscent of the chaotic behaviour of the classical double pendulum under free oscillations. Some results analogous to those presented in Figs 19b and 20a have been published, without discussion, by Ther & Kollár [60]. This adds confidence as to the validity of the herein reported results and suggests that the assessment of overturning risk of the (deterministic) system at hand in regions 1 and 2 might be possible only in a probabilistic sense.

It is worth stressing that the convergence study in Figure 6b does not necessarily cover the forced rocking case under earthquake excitation, or even the introduction of an extra block. For this reason, additional sensitivity studies were carried out (not shown in the interest of space) for the case of double block rocking and compared to the overturning map in Figure 19b. It was found out that the areas of the overturning regions are very similar - yet not identical - between the runs with time steps of 10^{-5} and 10^{-6} s (dimensionless time steps ω_g/p of about 10^{-5} and 10^{-4}, respectively). The small differences observed were naturally attributed to the chaotic nature of the 2 DOF rocking system (extreme sensitivity to initial conditions). In this light, it is unlikely that the details of the overturning maps will tend to stabilise with a gradually smaller timestep. For the purposes of this study, the time step of 10^{-6} s was considered adequate, in the sense that it demonstrates the "probabilistic" nature of overturning close to the boundaries of the various toppling modes, despite the purely deterministic nature of the problem. It is also fair to mention that special numerical formulations encompassing detection of "events" such as uplift and impacts, are available but they were not used in the study at hand.

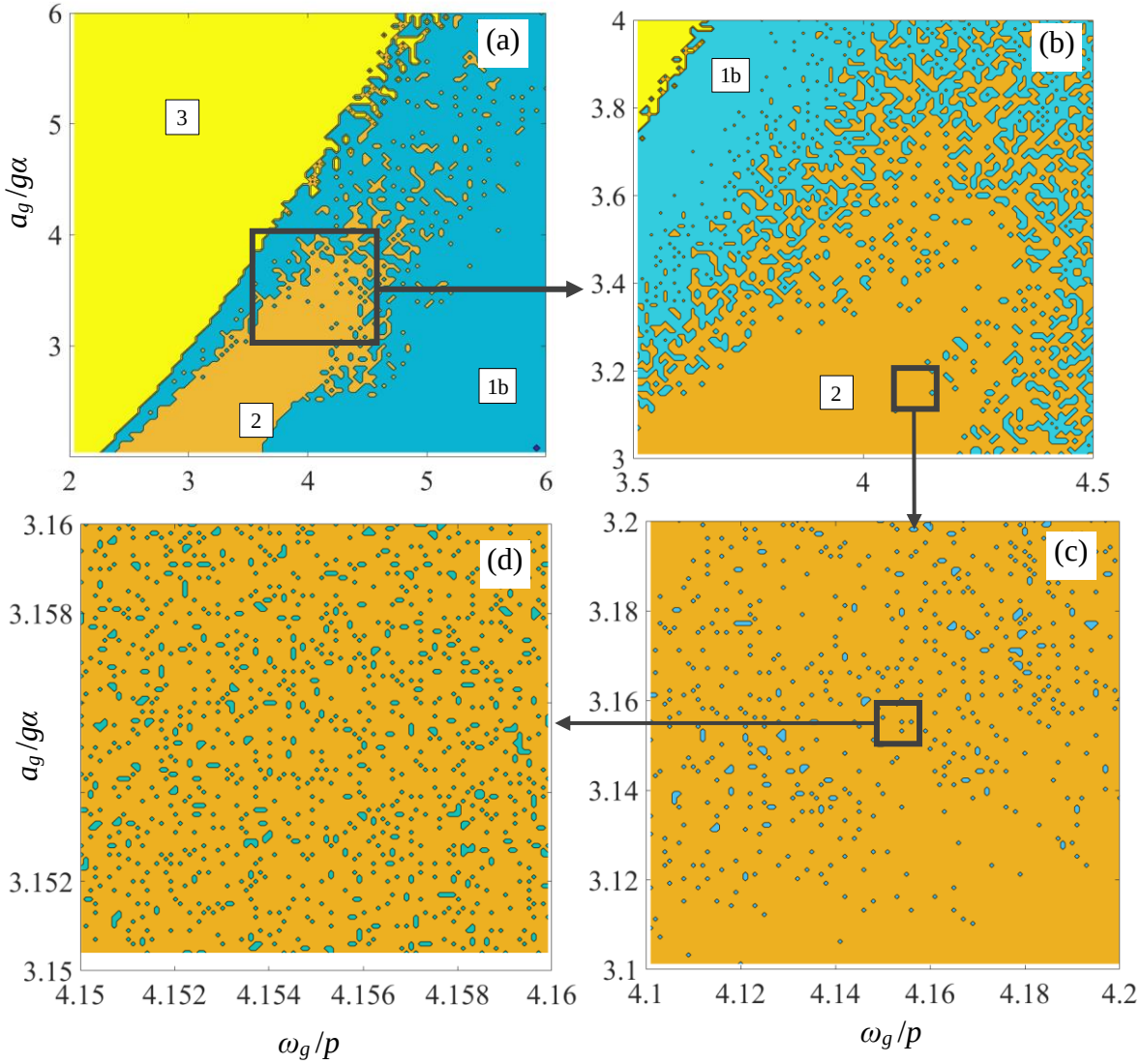

Figure 20: Magnifications of the fractal-like structure of Figure 19b, resulting from the impact model in Eq. (46).

The dependability of the time step used to produce the overturning map results can be further verified through the comparisons of Figure 24 (main text), where the overturning map interfaces of the literature are successfully predicted by the proposed algorithm, for both single and double block cases under harmonic ground excitation.

4 Discussion

4.1 Problem analysis & simulation

As shown in Figures 14 and 15, the computer algorithm underwent successfully the self-consistency tests, to verify the correctness and accuracy of the numerical results. Similar testing is not reported in the available literature, especially for the complex case of two or multiple blocks.

The final product of the approach introduced in the present study, using the binary indicators C_{R1} and C_{R2}, resulted in a numerical model which requires less than 20 lines of code to be programmed for the blocks motion and about 10 lines for each of the two impact cases of a double block system. This is a major advantage compared to classical approaches where the complexity of multiple equations for each case makes the debugging of the algorithm difficult, since the output is very sensitive to even the small errors/perturbations in initial conditions.

Furthermore, the present approach does not need additional mathematical expressions to model transition from one pattern to another, neither any constraint for the imposed momentum to start rocking motion. It was found that the derived model is capable to produce any dynamic behaviour of the block system in the realm of the original assumptions. Moreover, the present approach increases significantly the speed of the algorithm, since it eliminates the control commands that would be needed to separate several possible combinations of blocks' rotation and impact points.

4.2 Estimation of the experimental error

Based on the repeated experimental data sets shown in Figure 11, the accuracy of the measured block rotation angle lies within ±0.5º. The error in time measurements can also be extracted from this diagram, since it is only affected by the frame rate of recording. As can be observed, the average time error is of the order of 0.1 seconds, as the difference in time between same measured points of different sets varies between 0.05 and 0.15 seconds. The time error can become significant because whenever the block reaches maximum angular displacement the angular velocity becomes zero. Thus, the exact frame at which the block appeared to be at its maximum displacement could not always be precisely determined.

The deviation between the three sets of measurements is remarkably lower for block 1 and 3 (Fig. 12), which both have lower aspect ratio (b/h) than block 2 (Table 2). This behaviour can be explained considering that the various imperfections of the block and base surfaces affect more significantly the rocking and restitution behaviour of the shorter block 1, than that of the taller block 3.

Another source of experimental error may be the block weight and dimensions measurements, which are affected by the accuracy of the equipment employed in the tests. All the weight measurements of the blocks were made with an electronic scale of ± 0.025 kg accuracy, while the dimensions of each block were measured using a ruler of ± 1 mm accuracy. With that error in the length measurement, the error for the critical angle (α) is ± 0.6 degrees. Since all the

absolute errors are specified, they can be combined to determine a total absolute error in the calculation of $\ddot{\theta}$. For the case of free rocking motion equation (18) simplifies as follows:

$$\ddot{\theta} = \frac{4}{3R}[g\ sin(\alpha - \theta)] \quad (91)$$

Evidently, from equation (91) it emerges that the motion of a single block is independent of its mass and thus will be neglected in the error calculation. This can be explained by the fact that the angular velocity of the block, like that of a classical pendulum, is only affected by gravitational acceleration and the distance of the centre of mass from the point of rotation (R). Therefore, the expression of the absolute error for a function with more than one independent variable can be derived from a multivariable version of the Taylor series [66] and give the following relationship:

$$\Delta f(\tilde{x}_1, \tilde{x}_2, \dots, \tilde{x}_n) \cong \left|\frac{\partial f}{\partial x_1}\right| \Delta\tilde{x}_1 + \left|\frac{\partial f}{\partial x_2}\right| \Delta\tilde{x}_2 + \dots + \left|\frac{\partial f}{\partial x_n}\right| \Delta\tilde{x}_n \quad (92)$$

where n is the number of the independent variables, $\tilde{x}_1, \tilde{x}_2, \dots, \tilde{x}_n$ which have absolute errors $\Delta\tilde{x}_1, \Delta\tilde{x}_2, \dots, \Delta\tilde{x}_n$ respectively. For equation (91), n = 3, $\tilde{x}_1$ = R, $\tilde{x}_2$ = α and $\tilde{x}_3$ = θ.

Thus, from equations (91) and (92) it emerges that the absolute error for $\ddot{\theta}$ is ±1.4 rad/s^2 and hence the relative experimental error with respect to acceleration of gravity was estimated to be within ±14%. This is about the same order of magnitude as the experimental error stated by other researchers, who observed that identical experiments may produce quite different results, which are very sensitive to the initial conditions or minor perturbations. For example, the measurements of El-Gawady *et al.* [61], Kalliontzis *et al.* [68] were found to be repeatable with scattering while the measurements by Mouzakis *et al.* [48] were deemed non-repeatable.

4.3 Comparison between measurement and numerical results for single block

The agreement between the present numerical and experimental results shown in Figures 11 and 12 is quite satisfactory. The damping rate of both the amplitude and the period of block oscillation are well correlated. However, to achieve that, the coefficient of restitution taken by equation (23) had to be increased appropriately. According to previous studies [67, 68] this theoretical model does not represent a realistic scenario because it does not fulfil several of the initial assumptions. Since the blocks are not ideal, the side of contact will always have a small curvature and the impact may not occur at the corner point of the block. In their work, Schau and Johannes [64] showed that even a very small deviation from the ideal straight line results in remarkably higher values for the coefficient of restitution than predicted by the model.

The values for this coefficient as obtained from equation (23) and as corrected here are tabulated in Table 3 below. For the aspect ratio of the blocks used here, and for similar block/base materials, the obtained correction factors in Table 3 are similar to the ones obtained in other experimental works, as they are reported by Kalliontzis et al. [68]. These values are included, along with the present results, in Figure 20 that correlate the correction factor with the critical angle (or the aspect ratio) of the blocks. Moreover, Figure 20 shows that the correction factor of blocks 1-3 can be correlated with the critical angle (or the aspect ratio) of the blocks. It appears that the required correction factor increases with the critical angle of the block, which is approximated by a correction formula proposed by Kalliontzis et al. [68]. However, as the critical angle increases (> 0.3 rad), the measurements diverge significantly from this formula, because their dependency on the material of the block and the base increases. Thus, each material should be studied independently, especially for critical angles greater than

0.3 rad. Also note that the location of measurements for blocks 1-3 could also be affected by the estimated error of ±14% of Section 4.2.

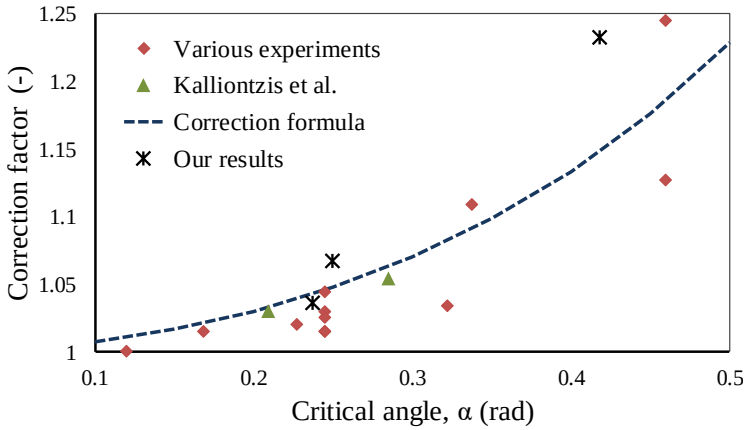

Figure 21: Relationship between the critical angle and the ratio of the correction in *r* and the measurements of Kalliontzis et al. [68].

Block	*r* (eq. 22)	Correct. factor	New r
1	0.9172	1.036	0.950
2	0.7527	1.233	0.928
3	0.9104	1.067	0.971

Table 3. Original and corrected coefficient of restitution with their corresponding factor

Concerning the forced excitation case, the comparison between experiments and calculations shown in Fig. 13 is again satisfactory. However, as can be observed in the measurements, there is a small divergence in the amplitudes of one side of rotation. This could be attributed to the systematic error of the transfer function of the table controller, which results in a non-symmetric amplitude output of the shaking table. The numerical algorithm predicts the time intervals between each peak successfully.

4.4 Two-blocks simulation and experimental results

From the comparative results of Fig. 16a it appears that the experimental points exhibit a remarkable discrepancy from the output of the algorithm, especially after the collision of the blocks. Nonetheless, this was expected due to the overestimation of the coefficient of restitution analysed above. Thus, it became apparent that the use of a correction factor was again necessary in order to match the experimental results with the ones obtained by the model. In this case however, such correction is not easy, because it affects the behaviour and the kinetic energy of both blocks, especially when after the first impacts the two blocks continue to move together.

As it can be observed in Figure 22, which represents an enlargement detail of Figure 15a, the angle variation of the upper and lower block is never identical, as many microscopic impacts constantly occur. In fact, for the duration of 0.24 to 0.55 seconds shown in Figure 22, the blocks collided for as many as 30 times. Even though these results need to be verified experimentally, it becomes apparent that there is no need for a special condition for keeping the blocks united. On the other hand, the dissipated kinetic energy at each impact, as predicted by the conservation of momentum model, causes additional reduction of kinetic energy and faster damping. But due to the large number of impacts, this restitution is not controllable and even small fixed correction factors may produce unrealistic results, or even destabilise the system altogether.

For this reason, a constant restitution coefficient is adopted for this case, the value of which was adjusted to improve the agreement of the numerical results with the measurements shown in Figure 16b (0.95 for the ground impact and 0.98 for the small impacts between blocks).

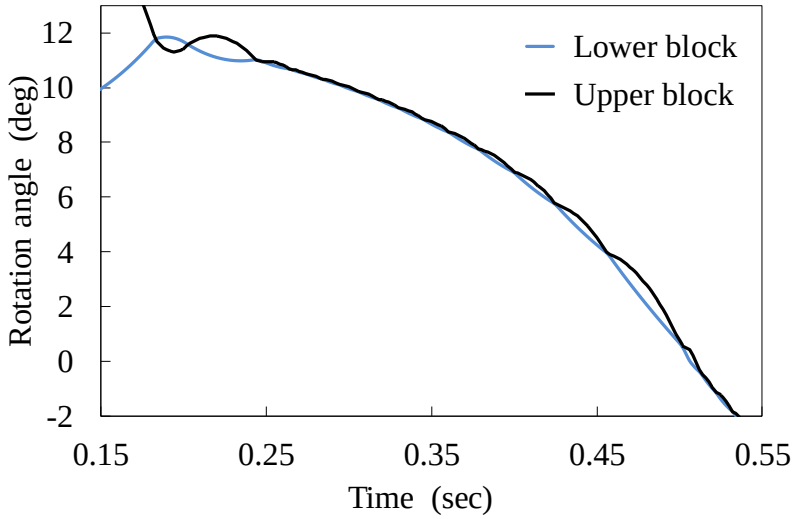

Figure 22: Magnification of rotation angle graph of Figure 15a.

As shown in Figure 17a, the numerical response for a sine acceleration wave of 7 Hz frequency and 3 mm amplitude agrees well with the experimental data, predicting the periodic motion, the amplitude and the phase difference (180^o) of the two blocks (though the measurements error for the lower block is high due to small angles). Moreover, this motion is established only after a few seconds, in both the laboratory tests and the algorithm results.

In Figure 17b, the numerical response for a sine wave of 5.5 Hz frequency and 3 mm amplitude reproduces well the behaviour observed in the tests for the same excitation conditions, namely very small angles of the lower block that eventually remains almost still, while the upper block obtains a periodic pattern. Figure 17c shows a similar behaviour but for a quite different combination of excitation frequency and amplitude, 3 Hz and 5 mm.

Finally, in Figure 17d the combination of 4 Hz/3 mm frequency/amplitude of the ground acceleration wave results in a complex non-periodic and non-symmetric response, with the upper block showing vibrations of higher rocking magnitude, and with some smaller periods of combined periodic motion of both blocks together. Such chaotic-like response was also observed in the experiments, although not for the same conditions (5 Hz, 5 mm)

The above results confirm the general behaviour of the force-excited two-block system, which was observed both experimentally and numerically, that the two-block system can have numerous different response patterns, periodic or not, and it is very sensitive to excitation conditions. Even a minor change of either the amplitude or the frequency of the external acceleration can cause an entirely different rocking motion pattern.

4.5 Overturning maps

As mentioned in section 3.3 (Fig. 18), for the single block rocking, the conservation of angular momentum model predicts more stable response of the block system than the use of corrected (increased) restitution coefficients. The latter, as expected, produce higher momentum of the

block after an impact, and hence, cause enlargement of the corresponding area 2 of the overturning maps (Fig. 18a).

The normalised stability characteristics of the two-block system shown in Fig. 19b is quite similar to that of single block (Fig. 18b), when the restitution is obtained from the conservation of angular momentum. However, the use of a constant corrected coefficient of restitution value of 0.92 for all impacts on the ground or between blocks seems to produce unrealistic results, especially regarding the overturning after an impact to the ground (region 2 in Fig. 19a). Indeed, such a consideration is arbitrary and there is no experimental evidence for the impacts of the two-block system. Also, the restitution coefficient of the lower block after an impact to the ground should depend on the relative position of the 2nd block above it, but for the impact between the blocks the restitution coefficient depends on their relative position and angular velocities as well.

The scattered areas in Fig. 19b are being enlarged for smaller slenderness angles α, namely for more slender blocks (higher y-values of the map). This is in agreement with the stability analysis of a rocking block motion under continuous excitation, made in [37], according to which, the boundary between stable and unstable regions becomes wider for lower damping, namely for higher values of the restitution coefficient, that correspond to more slender blocks (see also Table 3). On the contrary, the use of relatively small restitution coefficient of 0.92 for all impacts results in a much more stable behavior of the two-block system throughout the entire map of Fig. 19a.

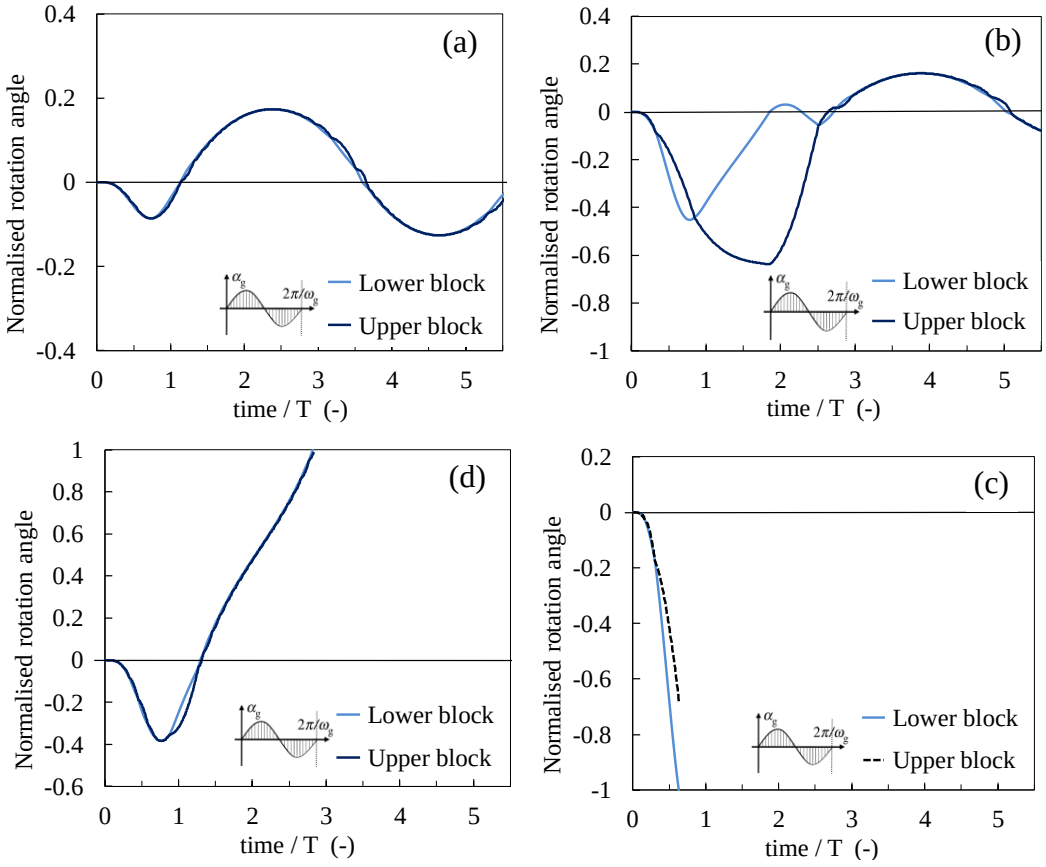

Figure 23: Indicative rocking trajectories from various regions of the overturning map for the two-block system (Fig. 19a): (a) →region 1a, (b) → 1b, (c) → 2, (d) → 3.

Similarly, the chaotic behaviour of the two-block system shown in the maps of Fig. 20, starts to appear above a certain value of normalised excitation amplitude (a_g/g a), that was also observed in [37] for continuous excitation of a single block. In the present case, this structure is probably created due to the impacts between the blocks that take place after the pulse, that may take place at quite different relative angles and restitution values for nearby points of the map, and hence the sensitivity to the excitation parameters becomes significant.

Figure 23 shows 4 indicative trajectories of the corresponding different regions of the double block system overturning map (Fig. 19a). The *y*-axis is normalised with the critical angle (α) and the *x*-axis is normalised by the period (T) of the single sinusoidal excitation pulse to be comparable. The lower block impacts on the ground when its curve crosses the line y=0, and the blocks are impacting one another when their curves intersect. The period of the sinusoidal pulse input is also shown in each graph.

In the stable region 1a (Fig. 22a) the blocks are rocking almost as a single object, with several minor impacts to each other (Fig. 22a), whereas in region 2a (Fig. 22b) the upper block deviates early due to its inertia and exhibits a trajectory to the opposite direction after its first impact on the lower block. However, after one or two such subsequent impacts, the system returns to that of an almost single object and shows a decaying rocking motion, as shown in region 1a. On the other hand, in the overturning regions 2 and 3 the two blocks move on the same direction and remain relatively close to each other for conditions that permit a first impact on the ground (Fig. 22c). However, for even stronger excitation amplitudes the upper block rotation is delayed due to its inertia, and hence the lower block overturns first (Fig. 22d).

4.6 Overturning map literature comparisons

The validity of the model was further verified by comparing several overturning map cases for one and two block systems with analytical and numerical results from the literature, as shown in Figure 24. The red points represent the result of the literature which are plotted on top of overturning maps produced by the algorithm of the study.

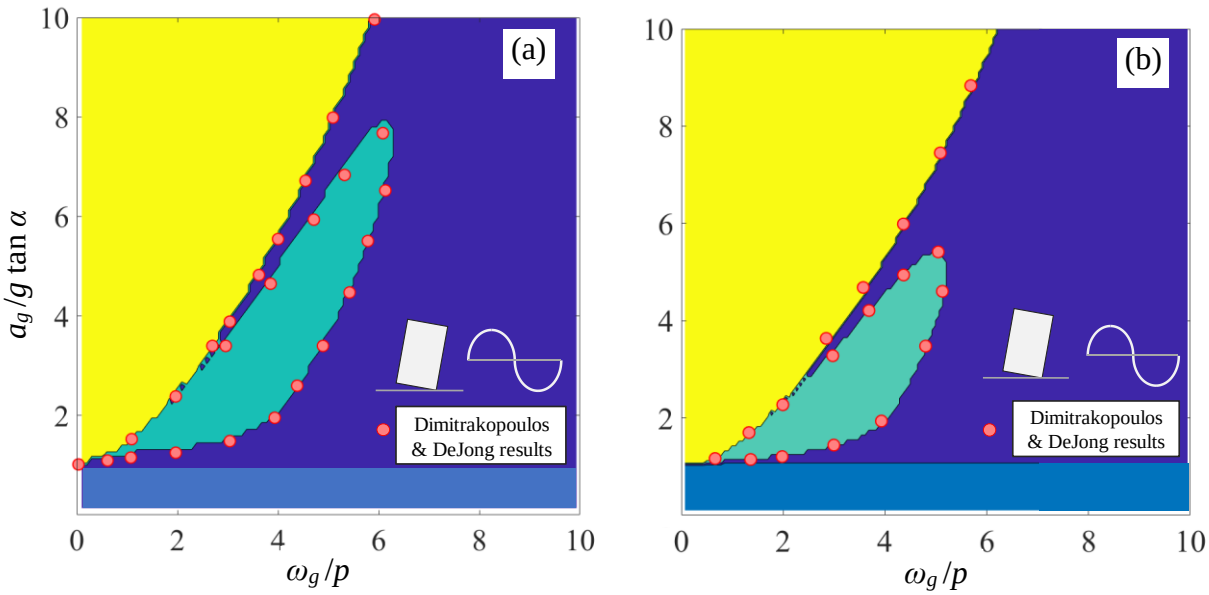

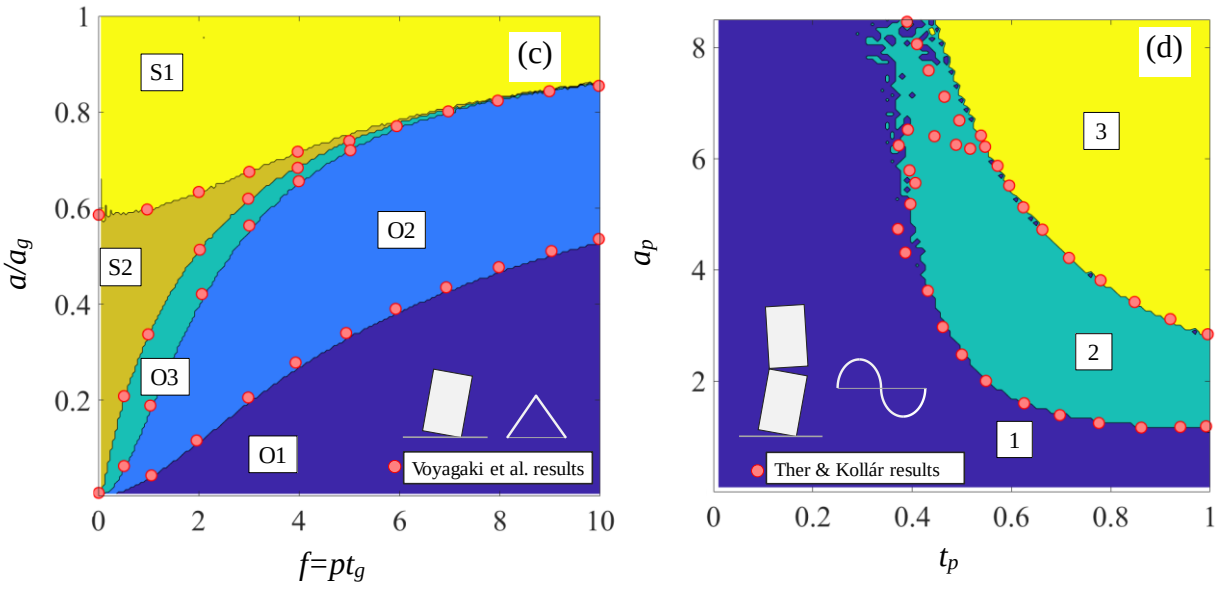

Figure 24: Overturning maps in comparison with the analytical results of Dimitrakopoulos & DeJong [28] (α = 20º, Fig. 24a, α = 5º Fig. 24b) and Voyagaki *et al*. [31] (α = 5º, Fig. 24c) and comparison with results of Ther & Kollár [60] (α = 9.46º, Fig. 24d).

Figures 24a, b and 24c represent the resulting overturning maps of a single block with either sinusoidal or triangular pulse excitation which are compared with points extracted from the analytical expressions of Dimitrakopoulos & DeJong [29] and Voyagaki *et al.* [31], respectively. The block critical angle α for Figures 24a and 24b is 20 and 5 degrees, respectively and the coefficient of restitution *r* is 0.85 in both cases and its regions are the same as in Figure 18. The results of Figure 24c concern a rocking block response with α = 5 degrees and *r = 0.85*. All three single block results are in good agreement with the results of the algorithm successfully predicting all the proposed regions and interfaces. The overturning map of Figure 24c has a triangular pulse with period TD and its regions are named as follows:

O1 = overturning before TD/2

O2 = overturning after TD/2 and before TD

O3 = overturning after TD

S1 = not. overturning, maximum displacement (angle) before TD

S2 = not overt., maximum displacement (angle) after TD

The results of the double block system are shown in Figure 24d, where the regions proposed by Ther & Kollár [60] are again plotted as points on top of the simulated results. The regions for this case are named as follows:

1 = stable decaying rocking of the block after the excitation pulse

2 = the block overturns after making one impact to the ground

3 = overturning without impacting the ground

It is worth mentioning that the model of Ther & Kollár [60] also addresses the block impacts using the cantilever approximation, which generally shows a satisfactory agreement with our closed-solution model derived by the angular momentum. However, the cantilever model shows an underestimation of the critical region, namely region 2 at x = 0.4 - 0.6 and y > 6, which could be attributed to the approximate nature of the impact model. Therefore, the results

produced by the exact solution of the conservation of angular momentum for each impact in the current study stand as a more rational approach.

5 Conclusions

In this paper, the dynamic behaviour during rocking motion of a single and a two rigid block system was investigated. The main stages and corresponding accomplishments of this study were the following:

a. Development of a compact mathematical model describing the equations of motion of one and two rocking blocks.
b. Derivation of a compact mathematical model describing the impact modes for up to two blocks (equivalent to Housner's expression for one block).
c. Development of a computer algorithm for numerical simulation of free and/or forced rocking of a block system with no additional condition (e.g. calculation of torques) to signify transfer between the equations of motion and impact.
d. Construction of a test platform in the laboratory and measure corresponding free and forced motion of rocking blocks.

Main conclusions gleaned from the study are:

(1) For both single-block and double-block systems the derivation of the mathematical model was divided in two parts: the equations of motion and the equations of impact. The final model can combine all possible relative positioning and motion of up to two blocks, into a single set of analytic expressions by the introduction of binary indicators (C_R). This is a significant advantage of the present approach compared to the literature that generalises the analysis which produces elegant final expressions and facilitates the numerical simulation, the validation of correctness as well as the accuracy of the results.

(2) The algorithm underwent several self-symmetry tests for single and double block rocking cases, in order to ensure that it is perfectly correct. This procedure revealed that the numerical results are very sensitive to even minor modelling discrepancies or programming errors.

(3) The numerical results were also validated experimentally for free and forced rocking motion of single and two-block systems. Repeatability was confirmed by several sets of measurements for each case, based on which the absolute error of the angle and time measurements was found to be $\pm 0.5^o$ and 0.1 sec, respectively. An error estimation method showed that the relative error in the angular acceleration was within ±14%, which is at about the same order of magnitude with other experimental works in the literature, and caused mainly by the sensitivity of the results on the initial and testing conditions.

(4) The coefficient of restitution of the single rocking block, as obtained by the angular momentum conservation model, had to be corrected in order to match the numerical results with the experiments, in accordance with the findings of other researchers. The correction factor was found to correlate with the aspect ratio of the rocking blocks.

(5) The two-block system subjected to horizontal sinusoidal acceleration showed a very complex, chaotic-like response, with numerous possible patterns that are very sensitive to the excitation conditions (amplitude and frequency).

(6) The developed model was finally used to produce normalised overturning maps for single and double-block systems, subjected to a single sinusoidal pulse, as an indicative application for realistic problems. Corrected restitution coefficients produced a much larger overturning-

after-impact region in single block maps, whereas in the two-block system the calculation of the angular velocity-dependent restitution also resulted in a remarkably different map topology. Map results for one and two block systems where compared and found to be in meaningful agreement with the literature.

(7) Following up on the above conclusion, the overturning map for the double block system revealed the existence of fractal-like regions, which can be interpreted in the context of deterministic chaos. Accordingly, the risk of overturning of multi-block systems can be evaluated only on a probabilistic sense, even for the strictly deterministic systems and the idealized excitations considered here. Such a probabilistic evaluation lies beyond the scope of this study.

ACKNOWLEDGEMENTS

The authors acknowledge the support of the technical staff at EQUALS laboratory at University of Bristol. The help of Dr. Elia Voyagaki in proofreading the manuscript and offering valuable suggestions is gratefully acknowledged. Finally, the comments by two anonymous reviewers helped improve the quality of the herein reported work.

6 References

[1] Kounadis A. N. (2015), On the rocking complex response of ancient multispondyle columns: a genious and challenging structural system requiring reliable solution, *Meccanica*, **50**, 261-292.
[2] Makris N. and Vassiliou M.F. (2015), The dynamics of the Rocking Frame, *Seismic Assessment, Behaviour and Retrofit of Heritage Buildings and Monuments, Computational Methods in Applied Sciences*, 37, Springer, 37-59.
[3] Milne J. (1885) Seismic experiments. *Transactions of the Seismological Society of Japan*; 8:1–82.
[4] Milne J, Omori F. (1893) On the overturning and fracturing of brick and columns by horizontally applied motion. *Seismological Journal of Japan*; 17:59–86.
[5] Kirkpatrick P. (1927) Seismic measurements by the overthrow of columns. *Bulletin of the Seismological Society of America*; 17:2.
[6] Richter C.F. (1958). *Elementary seismology*, W.F. Freeman & Company, San Francisco, and Bailey Bros. & Swinfen Ltd., London
[7] Muto K., Umemura H., Sonobe Y. (1960), Study of overturning vibration of slender structures. *2WCEE*, Tokyo, Japan.
[8] Housner G.W. (1963), The Behavior of Inverted Pendulum Structures during Earthquakes, *Bulletin of the Seismological Society of America*, **53**, 403-417.
[9] Yim C.S., Chopra A.K., Penzien J. (1980), Rocking response of rigid bodies to earthquakes, *EES*, **8**, 565-587.
[10] Aslam M., Salise DT., Godden W.G. (1980), Earthquake rocking response of rigid bodies, *Journal of Structural Division, ASCE*, **106** (2), 377-392.
[11] Tso W.K., Wong C.M. (1980), Steady state rocking response of rigid block, Part II: Experiments, *EESD*, **18**, 107–20.
[12] Ishiyama Y. (1982), Motions of Rigid Bodies and Criteria for Overturning by Earthquake Excitations, *Earthquake Engineering and Structural Dynamics*, **10**, 635-650.
[13] Psycharis I.N., Jennings P.C. (1983), Rocking of slender bodies allowed to uplift, *EESD*, **11**, 57-76.
[14] Spanos P.D., Koh A.S. (1984), Rocking of rigid bodies due to harmonic shaking, *Engineering Mechanics, ASCE*, **110** (11), 1627-1642.

[15] Makris N., Roussos Y. (1998), Rocking Response and Overturning of Equipment under Horizontal Pulse-Type Motions, Report PEER-1998/05, *Pacific Earthquake Engineering Research Center, College of Engineering*, University of California, Berkeley.
[16] Zhang J., Makris N. (2001), Rocking response of a free-standing blocks under cycloidal pulses. *Engineering Mechanics*, **127** (5), 473-48.
[17] Anooshehpoor A., Brune J.N., Zeng Y. (2004), Methodology for Obtaining Constraints on Ground Motion from Precariously Balanced Rocks, *BSSA*, **94** (1), 285-303.
[18] Prieto F., Lourenço P.B., Oliveira C.S. (2004), Impulsive Dirac-delta forces in the rocking motion, *EESD*, 33 (7), 839-857.
[19] Pena F., Prieto F., Lourenco P.B., Costa A.C., Lemos J.V. (2007), On the dynamics of rocking motion of single rigid-block structures, *Earthquake Engineering and Structural Dynamics*, **36**, 2383–2399.
[20] Vassiliou M. and Makris N. (2011), Analysis of the rocking response of rigid blocks standing free on a seismically isolated base, *Earthquake Engineering and Structural dynamics*, **41**, 177–196.
[21] Baratta A. and Corbi O. (2012), Analysis of the Dynamics of Rigid Blocks Using the Theory of Distributions, *Advances in Engineering Software*, **44**, 15-25.
[22] Dimitrakopoulos E. and DeJong M. (2012), Overturning of retrofitted rocking structures under pulse-type excitations, *Journal of Engineering Mechanics, ASCE*, **138**(8), 963–972.
[23] Psycharis I.N., Fragiadakis M., Stefanou I. (2013), Seismic reliability assessment of classical columns subjected to near-fault ground motions, *Earthquake Engineering & Structural Dynamics*, **42** (14), 2061-2079.
[24] Dejong M.J. and Dimitrakopoulos E.G. (2014) Dynamically equivalent rocking structures, *Earthquake Engineering & Structural Dynamics*, doi.org/10.1002/eqe.2410
[25] Dimitrakopoulos E.G. and Paraskeva T. (2015) Dimensionless fragility curves for rocking response to near-fault excitations, *Earthquake Engineering & Structural Dynamics*, doi.org/10.1002/eqe.2571
[26] Voyagaki E. and Vamvatsikos D. (2015), Probabilistic Assessment of Rocking Response for Simply-Supported Rigid Blocks, *SECED, Conference: Earthquake Risk and Engineering towards a Resilient World*, Cambridge, UK, 1-9 July.
[27] Giouvanidis A.I. and Dimitrakopoulos E.G. (2018) Rocking Amplification and Strong-Motion Duration, *Earthquake Engineering & Structural Dynamics*, DOI: 10.1002/eqe.3058
[28] Vassiliou M.F., Burger S., Egger M., Bachmann J.A., Broccardo M., Stojadinovic B. (2017), The three-dimensional behavior of inverted pendulum cylindrical structures during earthquakes, *Earthquake Engineering & Structural Dynamics*, **46** (14), 2261-2280.
[29] Dimitrakopoulos E.G. and DeJong M. (2012), Revisiting the Rrocking Block: Closed-form Solutions and Similarity Laws, *Proceeding of the Royal Society A*, **468**, 2294-2318.
[30] Voyagaki E. (2013), *Contributions to dynamic analysis of yielding systems to near-fault earthquake motions*, PhD Thesis, National Technical University, Athens, Greece
[31] Voyagaki E., Psycharis I.N. and Mylonakis G.E. (2013), Rocking Response and Overturning Criteria for free Standing Blocks to Single-lobe Pulses, *Soil Dynamics and Earthquake Engineering*, **46**, 85-95.
[32] Voyagaki E., Psycharis I.N. and Mylonakis G.E. (2014), Complex Response of a Rocking Block to a Full-Cycle Pules, *Journal of Engineering Mechanics*, **140**(6).
[33] Dimitrakopoulos E.G and Fung E.D.W. (2016) Closed-form rocking overturning conditions for a family of pulse ground motions, *Proceedings of The Royal Society A Mathematical Physical and Engineering Sciences*, DOI: 10.1098/rspa.2016.0662
[34] Kounadis A.N. (2013), Parametric study in rocking instability of a rigid block under harmonic ground pulse: A unified approach, *Soil Dynamics and Earthquake Engineering*, **45**, 125–143.
[35] Kounadis A.N. (2015), On the rocking–sliding instability of rigid blocks under-ground excitation: Some new findings, *Soil Dynamics and Earthquake Engineering*, **75**, 246–258.
[36] Psycharis I.N. (1990), Dynamic behavior of rocking two-block assemblies, *Earthquake Engineering and Structural Dynamics*, **19**, 555–575.

[37] Prieto F. and Lourenço P.B. (2005), On the rocking behavior of rigid objects, *Meccanica*, **40**(2), 121–133.
[38] Prieto F. (2007), *On the dynamics of rigid-block structures. Applications to SDOF masonry collapse mechanisms*, PhD Thesis, Universidade do Minho, Portugal.
[39] Hogan S.J. (1989), On the dynamics of rigid block motion under harmonic forcing, *Proceedings of the Royal Society of London A*, **425**, 441–476.
[40] Hogan S.J. (1992), Heteroclinic bifurcations in damped rigid block motion, *Proceedings of the Royal Society of London A*, **439**, 155–162, 1992.
[41] Spanos P.D., Roussis P.C., Politis P.A. (2001), Dynamic Analysis of Stacked Rigid Blocks, *Soil Dynamics and Earthquake Engineering*, **21**, 559-578.
[42] Sinopoli A. (1980), Dynamic evolution by earthquake excitation of multiblock structures, *Proc. Int.Conference on structural conservation of stone masonry: diagnosis, repair &strengthening*, Greek Ministry of Culture, Athens.
[43] Allen R.H., Oppenheim I.J., Parker A.P., Bielak J. (1986), On the dynamic response of rigid body assemblies, *Earthquake Engineering & Structural Dynamics*, **14**, 861–876.
[44] Papastamatiou D. and Psycharis I. (1993), Seismic response of classical monuments – a numerical perspective developed at the Temple of Apollo in Bassae, Greece, *Terra Nova*, **5**, 591-601.
[45] Winkler T., Meguro K., Yamazaki F. (1995), Response of rigid body assemblies to dynamic excitation, *Earthquake Engineering and Structural dynamics*, **24**, 1389-1408.
[46] Psycharis I.N., Papastamatiou D.Y., Alexandris A. (2000), Parametric investigation of the stability of classical columns under harmonic and earthquake excitations, *Earthquake Engineering and Structural Dynamics*, **29**, 1093–1109.
[47] Papantonopoulos C., Psycharis I.N., Papastamatiou D.Y., Lemos J.V., Mouzakis H. (2002), Numerical prediction of the earthquake response of classical columns using the Distinct Element Method, *EESD*, **31**, 1699–1717.
[48] Mouzakis H., Psycharis I., Papastamatiou D., Carydis P., Papantonopoulos C. and Zambas C. (2002), Experimental Investigation of the Earthquake Response of a Model of a Marble Classical Column, *Earthquake Engineering Structural Dynamics*, **31**, 1681-1698.
[49] Psycharis I.N., Lemos J.V., Papastamatiou D.Y., Zambas C., Papantonopoulos C. (2003), Numerical study of the seismic behaviour of a part of the Parthenon Pronaos, *EESD*, **32**, 2063–2084.
[50] Konstantinidis D. and Makris N. (2005), Seismic response analysis of multidrum classical columns. *EESD*, **34**, 1243–1270.
[51] Pena F., Lourenco P.B., Costa A.C. (2008), Experimental dynamic behavior of free standing multiblock structures under seismic loadings, *Journal of Earthquake Engineering*, **12**, 953–979.
[52] Dasiou M.E., Mouzakis H.P., Psycharis I.N., Papantonopoulos C., Vayas I. (2009), Experimental investigation of the seismic response of parts of ancient temples, *Prohitech conference*, Rome, 21–24.
[53] Papaloizou L. and Komodromos P. (2009), Planar investigation of the seismic response of ancient columns and colonnades with epistyles using a custom-made software, *Soil Dynamics and Earthquake Engineering*, **29**, 1437–1454.
[54] Ambraseys N., Psycharis I.N. (2011), Earthquake Stability of Columns and Statues, *J. Earthquake Engineering*, **15** (5), 685-710.
[55] Ambraseys N., Psycharis I.N. (2012), Assessment of the long-term seismicity of Athens from two classical columns, *Bulletin of Earthquake Engineering*, **10,** 1635-1666.
[56] Kounadis A.N., Papadopoulos G.J., and Cotsovos D.M. (2012), Overturning Instability of a Two-Rigid Block System Underground Excitation, *Journal of Applied Mathematics and Mechanics*, **92**, 536-557.
[57] Psycharis I.N., Fragiadakis M., Stefanou I. (2013), Seismic reliability assessment of classical columns subjected to near-fault ground motions, *Earthquake Engineering & Structural Dynamics*, **42** (14), 2061-2079.
[58] Kounadis A.N. (2014), Rocking instability of Free-Standing Statues atop Slender Viscoelastic Columns Under Ground Motion, *Soil Dynamics and Earthquake Engineering*, **63,** 83-91.

[59] Minafo G., Amato G. and Stella L. (2016), Rocking Behaviour of Multi-block Columns Subjected to Pulse-type Ground Motion Accelerations, *The Open Construction and Building Technology Journal*, **10**, 150-157.
[60] Ther T. and Kollár L.P. (2017), Model for multiblock columns subjected to base excitation, *Earthquake Engineering and Structural Dynamics*, **47**, 418-437.
[61] Voyagaki E, Kloukinas P, Dietz M, Dihoru L, Horseman T, Oddbjornsson O, Crewe AJ, Taylor CA, Steer A (2018) Earthquake response of a multiblock nuclear reactor graphite core: Experimental model vs simulations. *Earthquake Engineering and Structural Dynamics*, **47**(13): 2601-2626.
[62] Bachmann J.A., Strand M., Vassiliou M.F., Broccardo M., Stojadinović B. (2017), Is rocking motion predictable?, *Earthquake Engineering & Structural Dynamics*, **47** (2), 535–552.
[63] Giouvanidis A.I. and Dimitrakopoulos E.G. (2015) Seismic Response Analysis of the Planar Rocking Frame, *Journal of Engineering Mechanics*, 141(7), DOI: 10.1061/(ASCE)EM.1943-7889.0000939
[64] Giouvanidis A.I. and Dimitrakopoulos E.G. (2017) Seismic Performance of Rocking Frames with Flag-Shaped Hysteretic Behavior. *Journal of Engineering Mechanics* 143 (5), 04017008
[65] Zulli D., Contento A., Di Egidio A. (2012), 3D model of rigid block with a rectangular base subject to pulse-type excitation, *International Journal of Non-Linear Mechanics*, **47**, 679–687.
[66] Spanos P.D., Di Matteo A., Pirrotta A., Di Paola M. (2017), Rocking of rigid block on nonlinear flexible foundation, *International Journal of Non-Linear Mechanics* (Elsevier, in press).
[67] ElGawady M.A., Ma G., Butterworth J., Ingham J.M. (2006), Probabilistic Analysis of Rocking Blocks, *Proceeding of the New Zealand Society of Earthquake Engineering Conference*, New Zealand, Paper 17.
[68] Kalliontzis D., Sritharan S., Schultz A.E. (2017), Improving Accuracy of the Simple Rocking Model of Rigid Blocks, *Proceedings of the 16th world conference on Earthquake*, Santiago (Chile), Paper 451.
[69] Rajasekaran S. (2009), *Structural Dynamics of Earthquake Engineering*: Woodhead Publishing.
[70] Schau H. and Johannes M. (2013), Rocking and Sliding of Unanchored Bodies Subjected to Seismic Load According to Conventional and Nuclear Rules, *Proceedings of the 4th ECCOMAS conference on Computational Methods in Structural Dynamics and Earthquake Engineering*, Kos Island (Greece).
[71] Casapulla C. and Maione A. (2017), Free damped vibrations of rocking rigid blocks as uniformly accelerated motions, *International Journal of Structural Stability and Dynamics*, **17**, 6, 1750058.
[72] Chapra S.C. and Canale R.P. (1998), *Numerical Methods for Engineers*: WCB / McGraw - Hill.
[73] Kounadis A. N. and G. J. Papadopoulos (2016), On the rocking instability of a three-rigid block system under ground excitation, *Arch Appl Mech*, 86, 957-977.
[74] Kounadis A. N. (2018), The effect of sliding on the rocking instability of multi-rigid block assemblies under ground motion, *Soil Dynamics and Earthquake Engineering*, 104, 1-14.
[75] Kounadis A. N. (2019), Seismic instability of free-standing statues atop multispondyle columns: A heuristic very stable system of ancient technology, *Soil Dynamics and Earthquake Engineering*, **119**, 253-264.
[76] Makris N. and Konstantinidis D. (2003), The rocking spectrum and the limitations of practical design methodologies, *Earthquake Engineering and Structural Dynamics*, **32**, 265-289.
[77] Mylonakis G., Nikolaou S., Gazetas G. (2006), Footings under seismic loading: Analysis and design issues with emphasis on bridge foundations, *Soil Dynamics and Earthquake Engineering* **26**(9):824-853
[78] Kounadis A. N. (2015), New findings in the rocking instability of one and two rigid block systems under ground motion, *Meccanica*, **50**, 2219–2238.